



Bachelor Thesis

In Geoecology

University of Bayreuth

Micrometeorology Group

**Dynamics of the temperature and wind profiles in the  
boundary layer of a valley in the Fichtelgebirge  
Mountains**



*Author:* Elena Loos

*Supervisor:* Prof. Dr. Christoph Thomas

*Second Supervisor:* Dr. Wolfgang Babel

*November 28, 2016*

## Abstract

---

The atmospheric boundary layer is an important part of the atmosphere. In this 100 to 3000 m thick layer the atmosphere is affected by the surface of the earth. Processes in this part of the atmosphere such as the spreading of pollutants, the transfer of heat from the surface upwards or the transport of water vapor produced by transpiration and evaporation influence our lives importantly. This is why the understanding of these processes is crucial. In complex terrain there are additional processes such as up-valley and down-valley winds that occur due to slopes. The experiment “WOBLS” (Wind Observation in the Boundary Layer at the Schneeberg) aims at the better understanding of the wind flow and temperature distribution in the atmospheric boundary layer.

During a period of 40 days, wind direction and wind speed were measured by a SODAR (**SO**und **D**etection and **R**anging instrument) at the top of the Schneeberg in the Fichtelgebirge Mountains and wind direction, wind speed, potential temperature and the reflectivity of the antennas were measured by a SODAR RASS (**SO**und **D**etection and **R**anging instrument with **R**adio **A**coustic **S**ounding **S**ystem extension) at the bottom of the Schneeberg near the village Voitsumra. The measurements of the station at the bottom of every night and every day were used to identify different flow regimes in the area of the Schneeberg.

It was expected that the formation of a nightly inversion can be detected. Furthermore, the existence of low-level jets and cold air flow in combination with the development of cold air pools was expected. In addition it was planned to compare wind direction and wind speed of the station at the bottom and the summit-station.

It was found out that the main wind direction in this region is West. With low wind speeds there can be a change of wind direction with height from East at the bottom to South in a height of about 200 m agl. The stratification during most nights was stable, an inversion was detected in some of them. A low-level jet was observed in some nights, too. For cold air flows, the measuring range started too high, therefore a cold air flow could not be detected soundly. The maximum observational height was surprisingly low and the measuring ranges of the two stations did not overlap so a comparison was not made.

## Zusammenfassung

---

Die Atmosphärische Grenzschicht ist ein wichtiger Teil der Atmosphäre. Diese 100 bis 3000 m hohe Schicht ist dadurch charakterisiert, dass sie von der Erdoberfläche beeinflusst wird. Prozesse, die in dieser Schicht ablaufen, z.B. die Ausbreitung von Schadstoffen, der Transfer von Wärme von der Erdoberfläche aufwärts oder der Transport von Wasserdampf, der bei Transpiration und Evaporation gebildet wird, beeinflussen unser Leben stark, daher ist ein gutes Verständnis für diese Prozesse wichtig. In bergigem Gelände kommen aufgrund der Hangneigung weitere Prozesse, wie zum Beispiel Talauf- und abwinde, hinzu. Das Experiment "WOBLS" (Wind Observation in the Boundary Layer at the Schneeberg) zielt darauf ab, diese Vorgänge besser zu verstehen.

Während einer Messperiode von 40 Tagen wurden auf dem Gipfel des Schneebergs im Fichtelgebirge Windrichtung und Windgeschwindigkeit mit einem SODAR (**SO**und **D**etection **and** **R**anging) gemessen. Am Fuß des Schneebergs nahe dem Ort Voitsumra wurden mit einem SODAR RASS (**SO**und **D**etection **and** **R**anging Instrument mit **R**adio **A**coustic **S**ounding **S**ystem Erweiterung) Windrichtung, Windgeschwindigkeit, potentielle Temperatur und die Reflektivität der Antennen gemessen. Die Messwerte der Talstation der verschiedenen Tage und Nächte wurden genutzt um verschiedene Strömungsregime im Bereich des Schneebergs zu identifizieren.

Mit der Ausbildung einer nächtlichen Inversion wurde gerechnet. Außerdem wurde erwartet, dass man einen Low-level jet und Kaltluftabfluss erkennen kann. Verbunden mit dem Kaltluftabfluss wurde mit der Ausbildung eines Kaltluftsees gerechnet. Zusätzlich sollten die Windrichtungen und Windgeschwindigkeiten der Station auf dem Berg mit jenen der Station im Tal verglichen werden.

Die Hauptwindrichtung in dieser Region ist West, bei geringen Windgeschwindigkeiten Änderung der Windrichtung mit der Höhe von Osten am Boden zu Süden in einer Höhe von etwa 200 m. Die Schichtung der Atmosphäre war in den meisten Nächten stabil, an einigen davon wurde auch eine Inversion festgestellt. Ein Low-level jet war in einigen Nächten ebenfalls erkennbar. Für eine Beobachtung des Kaltluftabflusses begann der Messbereich zu weit oben, daher konnte der Kaltluftabfluss nicht zuverlässig festgestellt werden. Ein Vergleich

der beiden Stationen war nicht möglich, da die maximale Messhöhe überraschend niedrig war und es dadurch keinen überlappenden Messbereich gab.

# Table of Contents

---

Abstract .....	ii
Zusammenfassung.....	iii
Table of Contents .....	v
List of figures .....	vi
List of tables .....	viii
1. Introduction .....	1
<b>1.1. The Atmospheric Boundary Layer</b> .....	1
<b>1.2. Influence of Mountains on the boundary layer</b> .....	2
<b>1.3. Cold-air pooling</b> .....	3
2. Experimental Site.....	5
3. Material and Instruments .....	7
<b>3.1. Acoustic remote sensing</b> .....	7
<b>3.2. Mini SODAR at Station 1</b> .....	8
<b>3.3. SODAR RASS at Station 2</b> .....	9
4. Methods.....	10
<b>4.1. Classification of modes</b> .....	11
<b>4.2. Comparison of Station 2 and Station 1</b> .....	16
5. Results.....	18
6. Interpretation and Discussion.....	49
7. Conclusion.....	51
Literature.....	53
Appendix A: Additional tables and figures .....	54
Appendix B: Documentantation of location and settings.....	63
Acknowledgements.....	65
Declaration of Authorship .....	66

## List of figures

---

Figure 1: Map of the Basin „Weißenstädter Becken“ with the two measuring sites source: <a href="https://geoportal.bayern.de/bayernatlas/index.html?X=5551771.49&amp;Y=4489756.20&amp;zoom=8&amp;lang=de&amp;topic=ba&amp;bgLayer=tk&amp;catalogNodes=122">https://geoportal.bayern.de/bayernatlas/index.html?X=5551771.49&amp;Y=4489756.20&amp;zoom=8&amp;lang=de&amp;topic=ba&amp;bgLayer=tk&amp;catalogNodes=122</a> .....	5
Figure 2: Location of the SODAR RASS at station 2 and sketch of the arrangement of the SODAR RASS .....	6
Figure 3: Metek Sodar RASS at Station 2.....	9
Figure 4: Histogram of wind directions at 100 m agl during the day (upper one) and during the night (lower one).....	11
Figure 5: Histogram of differences of wind direction between 180 m agl and 60 m agl during the day (upper one) and during the night (lower one).....	12
Figure 6: Difference of wind direction between t and t+10 min versus wind speed at t at 100 m agl during the day (upper one) and during the night (lower one) and fitted loess-line (solid red line).....	13
Figure 7: Histogram of differences of temperature between 180 m agl and 40 m agl during the day (upper one) and during the night (lower one).....	14
Figure 8: Data availability in percent for direction (dir), temperature (temp), and wind speed (vel) during the day and during the night .....	15
Figure 9: Height profile of the route Schneeberg (Station 1) – Voitsumra (Station 2) source: <a href="https://geoportal.bayern.de/bayernatlas/index.html?X=5548413.90&amp;Y=4489535.34&amp;zoom=9&amp;lang=de&amp;topic=ba&amp;bgLayer=tk&amp;catalogNodes=122">https://geoportal.bayern.de/bayernatlas/index.html?X=5548413.90&amp;Y=4489535.34&amp;zoom=9&amp;lang=de&amp;topic=ba&amp;bgLayer=tk&amp;catalogNodes=122</a> .....	17
Figure 10: Height profile of the route Schneeberg (Station 1) – Voitsumra (Station 2) with height difference.....	17
Figure 11: Case 6, part 1 (n = 18) – On the left: ensemble-averaged time-height plots, on the right: height profile with standard deviation .....	18
Figure 12: Case 6, part 2 (n = 18) – On the left: ensemble-averaged time-height plots, on the right: height profile with standard deviation .....	19
Figure 13: Case 6 – Global solar radiation ( $K_{in}$ ) and net longwave radiation ( $I_{in} - I_{out}$ ) .....	21
Figure 14: Case 4, part 1 (n = 6) – On the left: ensemble-averaged time-height plots, on the right: height profile with standard deviation .....	22
Figure 15: Case 4, part 2 (n = 6) – On the left: ensemble-averaged time-height plots, on the right: height profile with standard deviation .....	23
Figure 16: Case 4 – Global solar radiation ( $K_{in}$ ) and net longwave radiation ( $I_{in} - I_{out}$ ) .....	24
Figure 17: Case 56, part 1 (n = 3) – On the left: ensemble-averaged time-height plots, on the right: height profile with standard deviation .....	25
Figure 18: Case 56, part 2 (n = 3) – On the left: ensemble-averaged time-height plots, on the right: height profile with standard deviation .....	26
Figure 19: Case 56 – Global solar radiation ( $K_{in}$ ) and net longwave radiation ( $I_{in} - I_{out}$ ) .....	27
Figure 20: Case 13, part 1 (n = 6) – On the left: ensemble-averaged time-height plots, on the right: height profile with standard deviation .....	28

Figure 21: Case 13, part 2 (n = 6) – On the left: ensemble-averaged time-height plots, on the right: height profile with standard deviation .....	29
Figure 22: Case 13 – downwelling longwave radiation ( $I_{in}$ ) and net longwave radiation ( $I_{in} - I_{out}$ ) .....	30
Figure 23: Case 15, part 1 (n = 5) – On the left: ensemble-averaged time-height plots, on the right: height profile with standard deviation .....	31
Figure 24: Case 15, part 2 (n = 5) – On the left: ensemble-averaged time-height plots, on the right: height profile with standard deviation .....	32
Figure 25: Case 15 – downwelling longwave radiation ( $I_{in}$ ) and net longwave radiation ( $I_{in} - I_{out}$ ) .....	33
Figure 26: Case 65, part 1 (n = 4) – On the left: ensemble-averaged time-height plots, on the right: height profile with standard deviation .....	34
Figure 27: Case 65, part 2 (n = 4) – On the left: ensemble-averaged time-height plots, on the right: height profile with standard deviation .....	35
Figure 28: Case 65 – downwelling longwave radiation ( $I_{in}$ ) and net longwave radiation ( $I_{in} - I_{out}$ ) .....	36
Figure 29: Case 18, part 1 (n = 3) – On the left: ensemble-averaged time-height plots, on the right: height profile with standard deviation .....	37
Figure 30: Case 18, part 2 (n = 3) – On the left: ensemble-averaged time-height plots, on the right: height profile with standard deviation .....	38
Figure 31: Case 18 – downwelling longwave radiation ( $I_{in}$ ) and net longwave radiation ( $I_{in} - I_{out}$ ) .....	39
Figure 32: Case 22, part 1 (n = 3) – On the left: ensemble-averaged time-height plots, on the right: height profile with standard deviation .....	40
Figure 33: Case 22, part 2 (n = 3) – On the left: ensemble-averaged time-height plots, on the right: height profile with standard deviation .....	41
Figure 34: Case 22 – downwelling longwave radiation ( $I_{in}$ ) and net longwave radiation ( $I_{in} - I_{out}$ ) .....	42
Figure 35: Case 38, part 1 (n = 2) – On the left: ensemble-averaged time-height plots, on the right: height profile with standard deviation .....	43
Figure 36: Case 38, part 2 (n = 2) – On the left: ensemble-averaged time-height plots, on the right: height profile with standard deviation .....	44
Figure 37: Case 38 – downwelling longwave radiation ( $I_{in}$ ) and net longwave radiation ( $I_{in} - I_{out}$ ) .....	45
Figure 38: Case 71, part 1 (n = 2) – On the left: ensemble-averaged time-height plots, on the right: height profile with standard deviation .....	46
Figure 39: Case 71, part 2 (n = 2) – On the left: ensemble-averaged time-height plots, on the right: height profile with standard deviation .....	47
Figure 40: Case 71 – downwelling longwave radiation ( $I_{in}$ ) and net longwave radiation ( $I_{in} - I_{out}$ ) .....	48

## List of tables

---

Table 1: Classification criteria for classifying the days and nights. The numbers in the brackets refer to the numbers in Table 3 and Table 5 in the appendix.....	10
Table 2: Categories of selected Cases .....	16
Table 3: Calculation of the classification for the different days starting with the 1 <sup>st</sup> of July as day 1 and ending with the 9 <sup>th</sup> of August as day 40 .....	54
Table 4: Sum of the days for all cases .....	55
Table 5: Calculation of the classification for the different nights starting with the night of 1 <sup>st</sup> to 2 <sup>nd</sup> July as night 1 and ending with the night of 9 <sup>th</sup> to 10 <sup>th</sup> August as night 40 .....	57
Table 6: Sum of the nights for all cases.....	58

# 1. Introduction

---

The WOBLS-Experiment (Wind observation in the boundary layer at the Schneeberg) aimed at observing wind systems in the complex terrain of the Fichtelgebirge Mountains. Therefore, measurements were made at the highest mountain in the Fichtelgebirge Mountains, the Schneeberg. The WOBLS-Experiment consists of two parts, one Station at the top of the Schneeberg at 1051 m a.s.l., in the following referred to as Station 1. The other Station is located north of the Schneeberg in a shallow basin at 585 m a.s.l. near the village Voitsumra, in the following referred to as Station 2. This site has direct visual contact to Station 1 at the Schneeberg. At Station 2, wind direction, wind speed and air temperature are measured with a Doppler **SO**und **D**etection and **R**anging instrument (SODAR) with RASS (**R**adio **A**coustic **S**ounding **S**ystem) extension. At Station 1 only wind direction and wind speed are measured with a Doppler **SO**und **D**etection and **R**anging instrument (SODAR). Wind speed, wind direction and air temperature of Station 2 are analyzed separately, and wind speed and wind direction of Station 2 and of Station 1 are compared additionally.

The wind systems and the temperature profiles that are analyzed are part of the Atmospheric Boundary Layer.

## 1.1. The Atmospheric Boundary Layer

The atmosphere expands to a height of about 500 km. But only in the lowest 11 km, the troposphere, the weather takes place (Wiedersich 2003). And only the first few kilometers react to processes at the surface of the earth. This boundary layer is about 100 to 3000 m high and is defined as the atmospheric layer that is directly influenced by the surface of the earth. Forces such as the frictional drag or processes like heat transfer, evaporation and transpiration, pollutant emission and terrain induced flow modification are important processes only appearing in the boundary layer. Most of the vertical transport in the boundary layer is caused by swirls of the air, called “Eddies” that exist in very different scales. These eddies are the reason for the interaction of the earth’s surface and the air above. The heat that is emitted by the earth because of the solar heating of the ground rises and forms eddies of medium size. Obstacles that deflect the air flow and the frictional drag of the ground cause eddies of similar size. These eddies generate smaller eddies, transferring turbulence energy

from the larger to the smaller eddies. This transfer of turbulence energy is called “energy cascade”. In the end, the energy of the smallest eddies is dissipated into heat by molecular viscosity.

The boundary layer has its very own stratification which also differs from day to night. During the day the boundary layer consists mostly of a mixed layer. Mixing of moisture, heat and pollutants in this layer is mostly convectively driven. Also momentum can be transported to the surface from the free atmosphere where no frictional drag slows down the wind speed. This increases the wind speeds in the mixed layer near the surface. The solar radiation heats the ground and as a result the air above. These rising thermals mix the air above the surface. Cold air sinking down from low clouds that are sometimes forming the top of the mixed layer can do the same. But also advective mixing can occur, especially when the wind is strong. A capping stable layer, the entrainment zone, forms the border of this turbulent mixing layer. It grows by entraining of air from the non-turbulent atmosphere above. About half an hour before sunset the rising of warm thermals stops because of the missing solar radiation. The existing mixed layer remains as it is, now neutrally stratified as there is no convectively driven turbulence anymore. This layer is called residual layer during the night. Because of the influence of the earth’s surface, which cools down and leads to a cooling of the air near the surface, the layer directly above the ground is transformed to a stable stratified layer. This layer is called the stable boundary layer. Wind speeds in the night mostly slow down in the stable boundary layer because there is no momentum transport to the surface anymore, but higher wind speeds can occur above at about 200 m, forming so called low-level jets or nocturnal jet. Cold air at ground level however begins to flow downhill under the influence of gravity, collecting in hollows. When the sun rises, the rising thermals begin to form, dissolving the stable boundary layer from below (Stull 2009; Oke 1978).

### **1.2. Influence of Mountains on the boundary layer**

In complex terrain the wind systems and atmospheric conditions are different at exposed ridge tops and shielded valleys: on ridge tops the influence of regional airflows is greatest whereas in the valleys the influence of the topography is greatest. At lower elevations negative lapse rates, thus a decrease of potential temperature with height, are associated with stable atmospheric conditions, calm winds and clear sky conditions. Positive lapse rates, thus an increase of potential temperature with height, in contrast mostly go together with

unstable conditions, overcast sky and strong winds. The wind systems in mountainous terrain often follow a special scheme, driven by differences in the heating of the surface because of different exposure to the solar radiation. Slopes oriented to the east get heated earlier than the surface of the valley's floor or slopes oriented to the west. This results in air flows driven by differences of air temperature and therefore air pressure. Geiger et al. (2009) refer to these air flows as an active topographic effect. In contrast, the influence is described as a passive topographic effect when existing regional air flows are modified by the dynamic influence of slopes and hills. These mountainous wind systems caused by temperature differences can be divided into four different interacting systems. The first one is the system of the down- and upslope winds. The second system is formed by the along-valley winds. These winds change direction in a diurnal pattern. They blow downslope and down-valley in the nights and upslope and up-valley during the days. When the sun rises, first the slope winds begin to change direction downslope (katabatic) to upslope (anabatic) because the slopes are heated by the solar radiation first, then followed by the down-valley winds changing to up-valley. Shortly before sunset, when net radiation changes from negative to positive due to the missing solar radiation, the directions change from anabatic to katabatic, again starting with the slope winds. The third wind system is the cross-valley flow, blowing from the slope that is heated stronger to the cooler one. These winds are mostly weak. The mountain-plain wind, which is the fourth wind system, blows from great plains up the mountain sides during the day and from the mountain down to the plain during the night (Whiteman 2000; Geiger et al. 2009).

### 1.3. Cold-air pooling

The cooling of air above the earth's surface is tied to the radiation balance which can be described by:

$$Q^* = K \uparrow + K \downarrow + I \uparrow + I \downarrow \quad (1)$$

Where  $Q^*$  is the net radiation,  $K \downarrow$  is the global solar radiation,  $I \downarrow$  is the downwelling longwave radiation that is emitted by the atmosphere,  $I \uparrow$  is the surface radiation, the longwave radiation that is outgoing from the surface and  $K \uparrow$  is the reflected solar radiation, the shortwave radiation that is reflected by the earth's surface. Per definition, the downward fluxes are negative and the upward fluxes are positive. The global solar radiation  $K \downarrow$  can be divided in:

$$K \downarrow = S + D \quad (2)$$

With  $S$  as the direct-beam solar radiation, that is not reflected by clouds or absorbed or scattered by the atmosphere and  $D$  as the diffuse solar radiation that is scattered by clouds or the atmosphere. During the night,  $S$ ,  $D$  and  $K \uparrow$  are zero, which leads to  $Q^* = I \uparrow + I \downarrow$ . Since  $I \uparrow$  is normally larger than  $I \downarrow$  and  $I \downarrow$  is defined as negative,  $Q^*$  is almost always positive. A positive  $Q^*$  means that the flux is directed upward. That means there is a net loss of radiation at night so the earth's surface cools down in the evening. Air in contact to the cool surface cools down. Because of the cold air being denser than the warmer air above, it begins to flow downhill on a sloped surface. These flows are called nocturnal cold air currents, they occur only at calm conditions. Cold air currents are small and therefore easily disturbed by higher wind speeds. With increasing slope, the air currents get stronger. Down flowing cold air accumulates in hollows, enclosed basins without a drainage outlet, forming cold air lakes (Stull 2009; Geiger et al. 2009).

#### 1.4. Objectives and Hypotheses

Three main objectives should be treated in this study. The first objective is the observation of the temperature profile at station two. It is expected that the formation of a stable boundary layer with a stable stratification can be observed. In nights with low wind speeds the building of an inversion should be detected, caused by the cold air flowing down from the Schneeberg combined with the radiative cooling of the surface. In nights with high wind speeds it is expected that the formation of a stable boundary layer is disturbed. During the days the stratification is supposed to be neutral or unstable. The second objective is the observation of the wind system. Due to the surrounding mountains the wind direction is expected to be influenced by these obstacles. The wind direction is supposed to be West in cases where there are high wind speeds, because westerly synoptic winds are blowing from high-pressure areas to low-pressure areas in the zone of the Westerlies (Malberg 2007). When the wind speeds are low, an influence of the surrounding mountains should be detected. The wind is expected to blow upslope the Schneeberg, therefore blowing from North, during the days. During the nights, the wind is expected to blow downslope from the Schneeberg, therefore blowing from South. In the nights, when there is a stable boundary layer in the basin, a decoupling from the layer above is supposed to cause different wind directions in the two layers. The third

objectives is the comparison of the wind systems at station 1 and station 2. It is expected that the wind directions are similar at both stations indicating a connection of both wind systems.

## 2. Experimental Site

The Metek SODAR RASS at Station 2 was set up at 585 m above sea level (a.s.l.) on a field near Voitsumra in the district Wunsiedel im Fichtelgebirge in the northeastern part of Bavaria, Germany (see Figure 2). It has direct visual contact to the top of the Schneeberg, the highest Mountain in the Fichtelgebirge Mountains, where the Scintec mini SODAR of Station 1 was placed. Voitsura lays at the edge of the “Weißenstädter Becken”, a basin surrounded by several mountains with an altitude between 780 and 880 m a.s.l. and the Schneeberg with an altitude of 1051 m a.s.l. (see Figure 1). In the east, the basin is open with no surrounding hills.

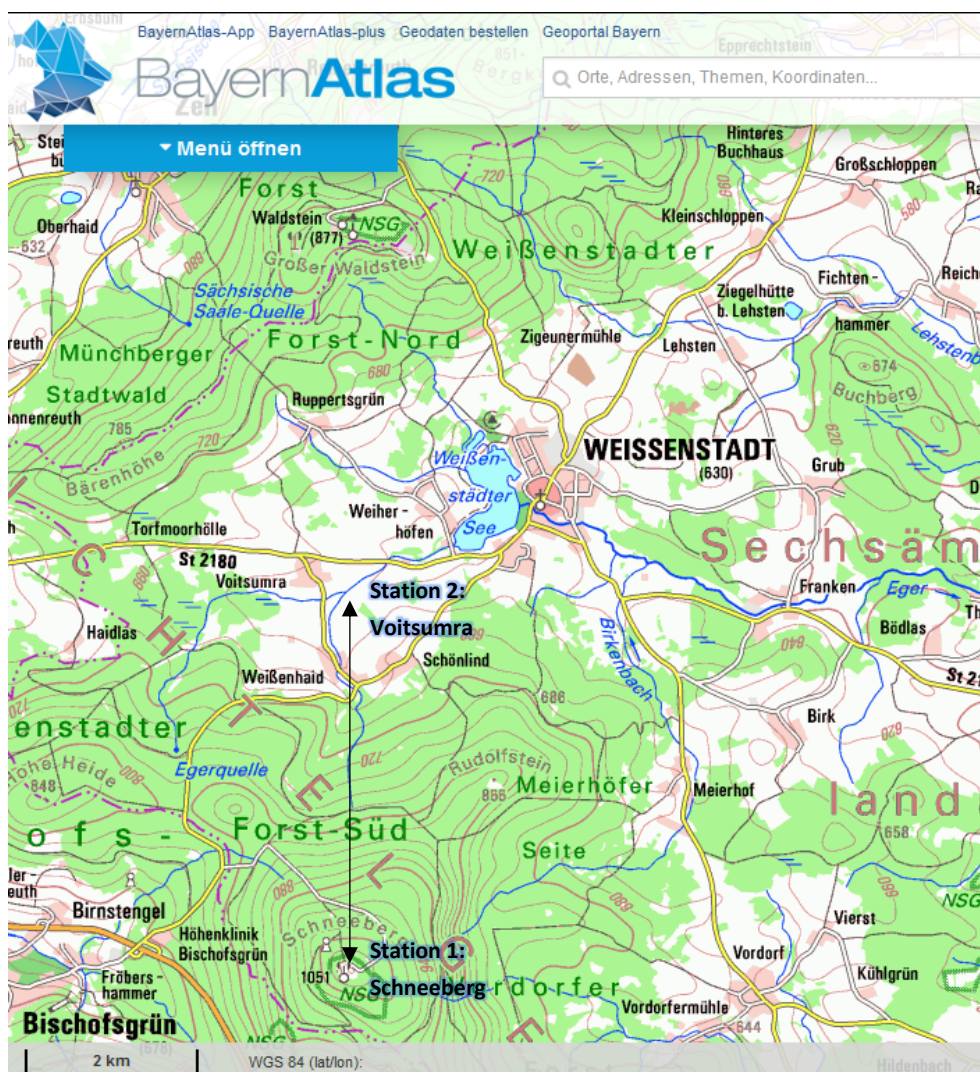


Figure 1: Map of the Basin „Weißenstädter Becken“ with the two measuring sites

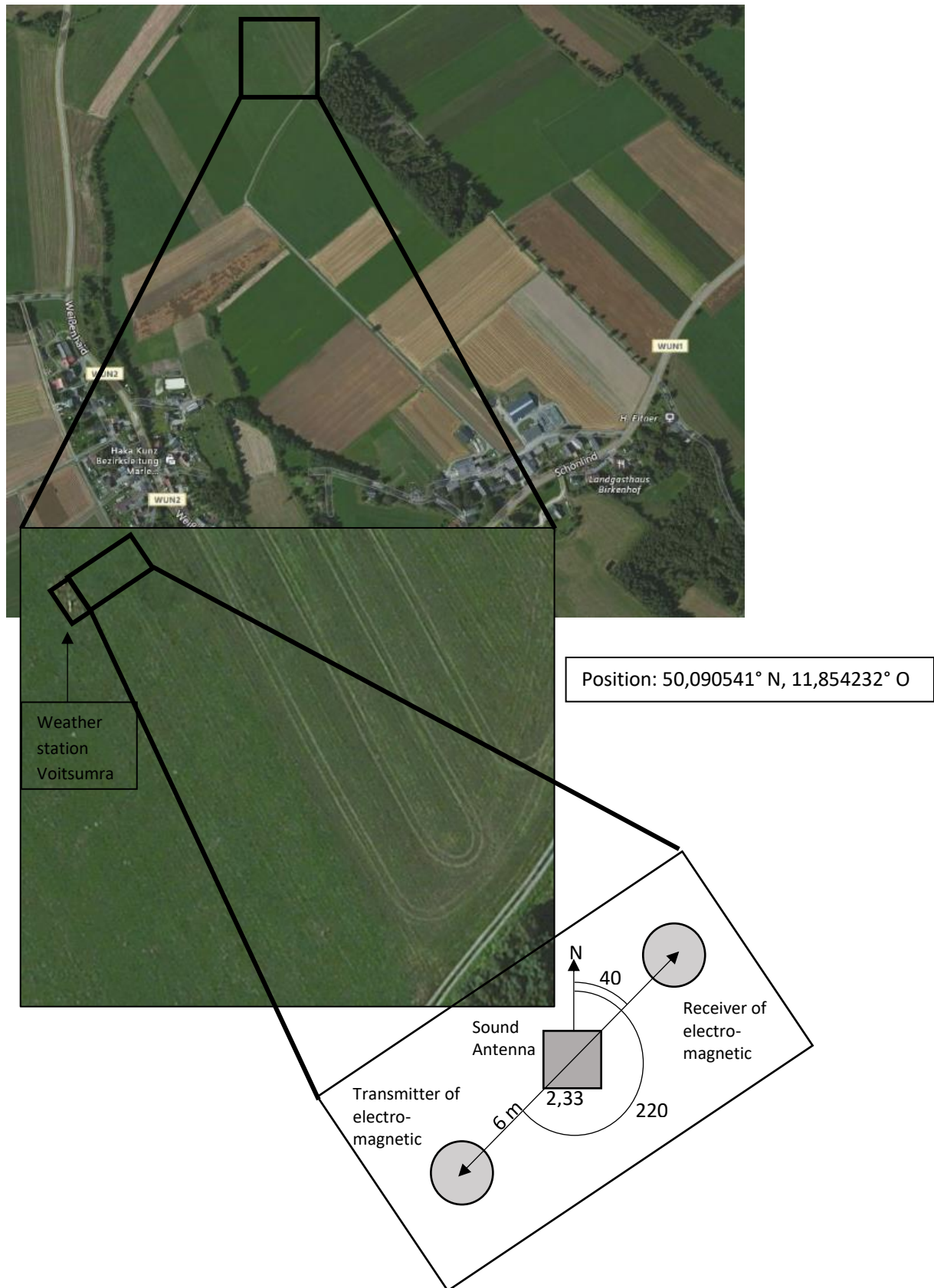


Figure 2: Location of the SODAR RASS at station 2 and sketch of the arrangement of the SODAR RASS

## 3. Material and Instruments

---

### 3.1. Acoustic remote sensing

For measuring wind speed and wind direction at Station 1, a Doppler SODAR is used. The sound antenna sends sound pulses that are scattered back by density inhomogeneities in the air. Due to the Doppler Effect the frequency of the received scattered signal is shifted from the emitted frequency. The Doppler Effect states that sound waves are compressed or stretched, if the reflecting density inhomogeneities move towards the antenna or away from it respectively. With Equation (3) the wind velocity in the direction of the emitted sound beam can be calculated.

$$f_s = f_0 * \left(1 - \frac{2v_r}{c}\right) \quad (3)$$

Where  $f_s$  is the frequency of the received signal,  $f_0$  is the frequency of the emitted sound pulse,  $v_r$  is the wind velocity in the direction of the emitted sound beam and  $c$  is the adiabatic speed of sound (Singal 1997).

By using a three-component SODAR that emits the sound pulses in three different directions, the whole vector of wind velocity can be determined. The sound pulse is sent straight up, to the north or to the south at an oblique angle and to the east or to the west at an oblique angle. The height of the moving inhomogeneity can be calculated by measuring the traveling time of the sound pulse. The inhomogeneities have to fulfill Bragg's law, resulting in the fact, that only eddies with a scale of about half of the wavelength can be detected.

$$l_t = \frac{\lambda}{2 * \sin \Theta_B} \quad (4)$$

Where  $l_t$  is the scale of the inhomogeneities,  $\lambda$  is the length of the sound waves and  $\Theta_B$  is the angle of wave incidence (the Bragg angle).  $\Theta_B$  is half of the scattering angle  $\theta$ .

For measuring temperature and wind profile at Station 2, a Doppler SODAR with RASS extension was used. Two radar antennas are placed at both sides of the SODAR (see Figure 2), providing the possibility to measure the temperature. The RASS-antenna continuously sends an electromagnetic wave at 1290 kHz while the other one is receiving the backscatter. The electromagnetic pulses are scattered back at the sound beams of the SODAR. While the sound

pulses travel with the speed of sound, the electromagnetic waves travel with the speed of light. The frequency of the received scattered electromagnetic signal is shifted from the frequency of the emitted signal. With the measured frequency-shift and the wavelength of the electromagnetic waves, the speed of sound can be calculated by (Singal 1997):

$$\delta f = \frac{2c_a}{\lambda_e} \quad (5)$$

Where  $\delta f$  is the measured frequency-shift,  $\lambda_e$  is the wavelength of the electromagnetic waves and  $c_a$  is the sound velocity. The sound velocity depends on the air temperature and the humidity. In dry air and within ideal gas approximation the relation between sound velocity and virtual temperature is

$$T_v = \left( \frac{c_a}{20,04} \right)^2 \quad (6)$$

Where  $T_v$  is the virtual temperature in Kelvin and  $c_a$  is the speed of sound. Like this, the virtual Temperature can be calculated (Singal 1997).

The soundwaves have to fulfill the Bragg-condition, too: the wavelength of the sound waves has to be half of the wavelength of the electromagnetic waves. The Metek SODAR RASS is sending out electromagnetic waves with a frequency of 1290 kHz. Fulfilling the Bragg-condition, the wavelength of the sound pulse that is sent out to scatter the electromagnetic waves has to be 2900 kHz (Metek 1999).

### 3.2. Mini SODAR at Station 1

The Mini SODAR at Station 1 was a SFAS (small Scintec Flat Array Sodar) Doppler SODAR from Scintec. It consists of 64 piezo-electric loudspeakers, forming an array of eight times eight loudspeakers. They are shielded by an octagonal enclosure that also protect the people around it from the sound pulses of the loudspeakers. The array of loudspeakers is used as a logical antenna that can emit sound beams to nine different directions. One is oriented upwards and always two are oriented to the north, to the east, to the south and to the west, at an angle of 19° and 24° respectively (Scintec AG 2016).

Recording of data started at 10 m above the ground and data is recorded every 5 m until 495 m. The distance between two measuring heights is called gate.

### 3.3. SODAR RASS at Station 2

The SODAR RASS was a Doppler-SODAR DSDPA.90/64 with 1290 MHz RASS-Extension, both from Meteorologische Messtechnik GmbH (Metek) (see Figure 3). The SODAR consists of 64 loudspeakers forming an array of eight times eight loudspeakers. They act as transmitters and receivers at the same time forming a monostatic SODAR. The array of loudspeakers is used as a logical antenna that sends the sound pulses to five different directions, straight up, to the north, to the east, to the south and to the west. The angle at which the sound beams are emitted is determined by the frequency that is chosen, it is about 30°. Two enclosures shield the loudspeakers from the noises of the environment and protect the people from the sound pulses of the loudspeakers. The RASS-Extension consists of two additional antennas that are placed on both sides of the SODAR. One of the RASS-antennas is the transmitter and the other one the receiver. A temperature sensor (PT100) was mounted at one of the RASS-antennas serving as a reference thermometer (Metek 1999).

Measurements started at the 1st of July and ended at the 10th of August. Hence, the data set that is analyzed contains 40 days and 40 nights. The recorded Data starts at a height of 40 m agl and ends at a height of 600 m agl, the gates spacing here is 20 m. Data is collected about every 4 seconds. As Mein data the average of 10 minutes is used. The frequency of the sound waves was first 1900 kHz but was changed to 1600 kHz when it was evident that the lower frequency achieved better results.



Figure 3: Metek Sodar RASS at Station 2

## 4. Methods

---

From the data that was collected by the METEK SODAR RASS at station 2, the values for wind direction, wind speed, standard deviation of the vertical wind speed ( $\sigma_w$ ) and potential temperature were analyzed. Furthermore, the reflectivity of the third antenna, which points upwards and the reflectivity of the RASS-antenna that sends the sound waves where the electromagnetic waves are reflected were analyzed. The values with a poor signal-to-noise ratio were dismissed with the program METEK graphics software. The data sets for the 40 days were split into 80 files of one day (8:00 till 19:50) or one night (20:00 till 07:50) respectively for each variable that was analyzed. These files contain 72 values each (10-minute-averages \* 6 times 10 minutes per hour \* 12 h). For each 10-minute step, there are values for 28 different heights, starting at 40 m agl and ending at 600 m agl with a spacing of 20 m. If the signal-to-noise ratio was too poor, a NA for “Not Available” was set instead of a value. The days and nights were classified into different categories by wind direction at 100 m agl, difference of wind direction between 180 m agl and 60 m agl, velocity at 100 m agl and difference of temperature between 180 m agl and 40 m agl (see table Table 1). For each day and night, according to the availability at the height that is specified in Table 1, it was calculated into which class they fall. The available time steps, that were not NA, are referred to as “cases” in 4.1.

**Table 1: Classification criteria for classifying the days and nights. The numbers in the brackets refer to the numbers in Table 3 and Table 5 in the appendix.**

Criteria	Classification			Elevation
Wind direction	West (= 1)	East (= 2)	Not differentiated (ND = 3)	100 m agl
Difference of Winddirection	Absent (= 1)	Present (= 2)	ND (= 3)	Comparing 180 m agl and 60 m agl
Velocity	Weak (= 1)	Strong (= 2)	ND (= 3)	100 m agl
Stratification	Unstable & Neutral (= 1)	Stable (= 2)	ND (= 3)	Comparing 40 m agl and 180 m agl

#### 4.1. Classification of modes

##### Wind direction at a height of 100 m agl

- West: 220° - 300° in more cases than in the classes “east” and “not differentiated” together.
- East: 50° - 100° in more cases than in the classes “west” and “not differentiated” together.
- Not differentiated (ND): 301° - 49° or 101° - 219° in more cases than in the classes “west” and “east” together, or, if none of the classes “west”, “east” or “ND” is true.

The limits were set at points where there was an apparent break in the Histogram of wind directions at 100 m agl (see Figure 4).

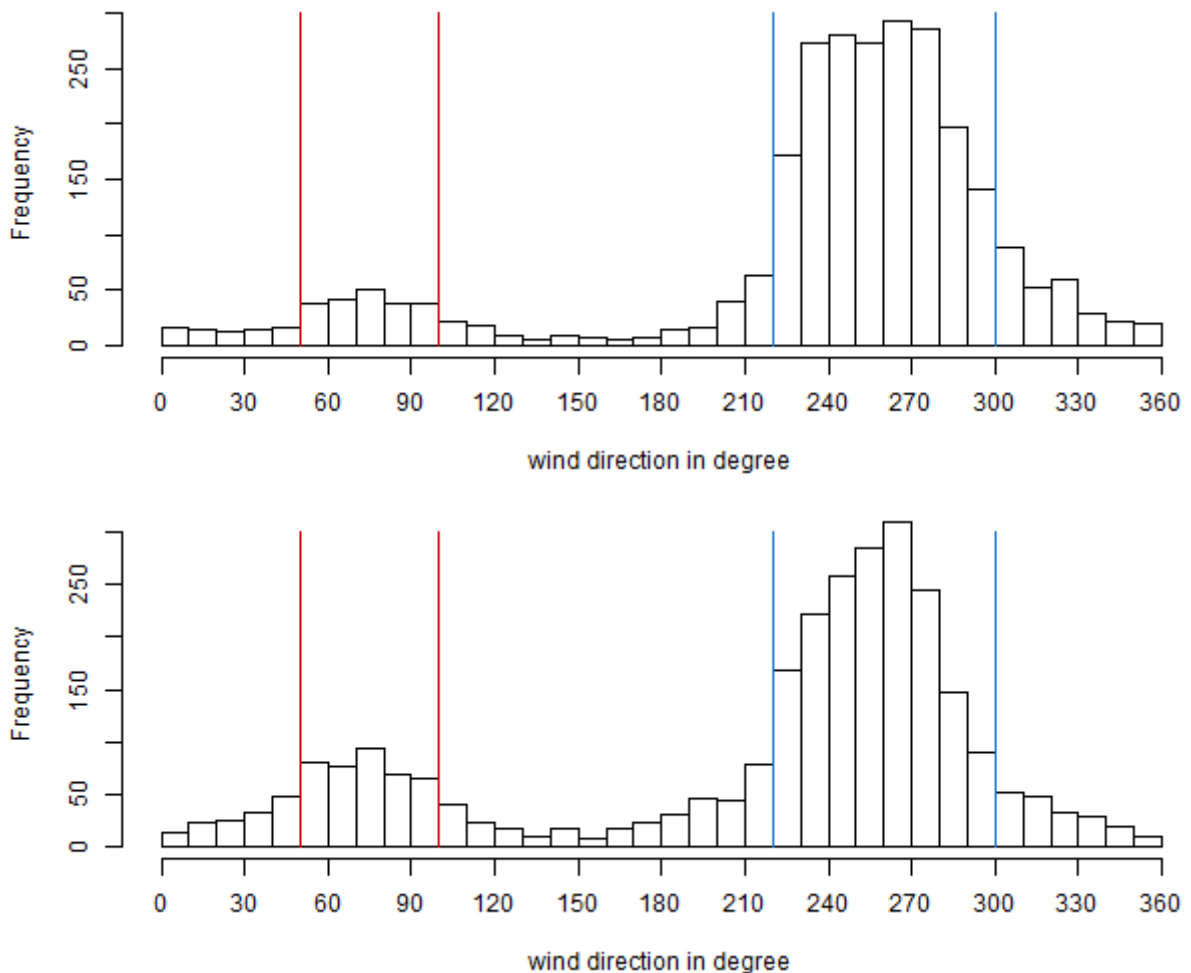


Figure 4: Histogram of wind directions at 100 m agl during the day (upper one) and during the night (lower one)

### Difference of wind direction between 180 m agl and 60 m agl

- Absent: the difference is  $\leq 14^\circ$  during the day and  $\leq 28^\circ$  during the night in more than twice as much cases as in the class “present”.
- Present: the difference is  $> 14^\circ$  during the day and  $> 28^\circ$  during the night in more than twice as much cases as in the class “absent”.
- Not differentiated (ND): none of the classes “absent” or “present” is true.

The limits were set at points where there was an apparent break in the Histogram of differences of wind direction between 180 m agl and 60 m agl (see Figure 5).

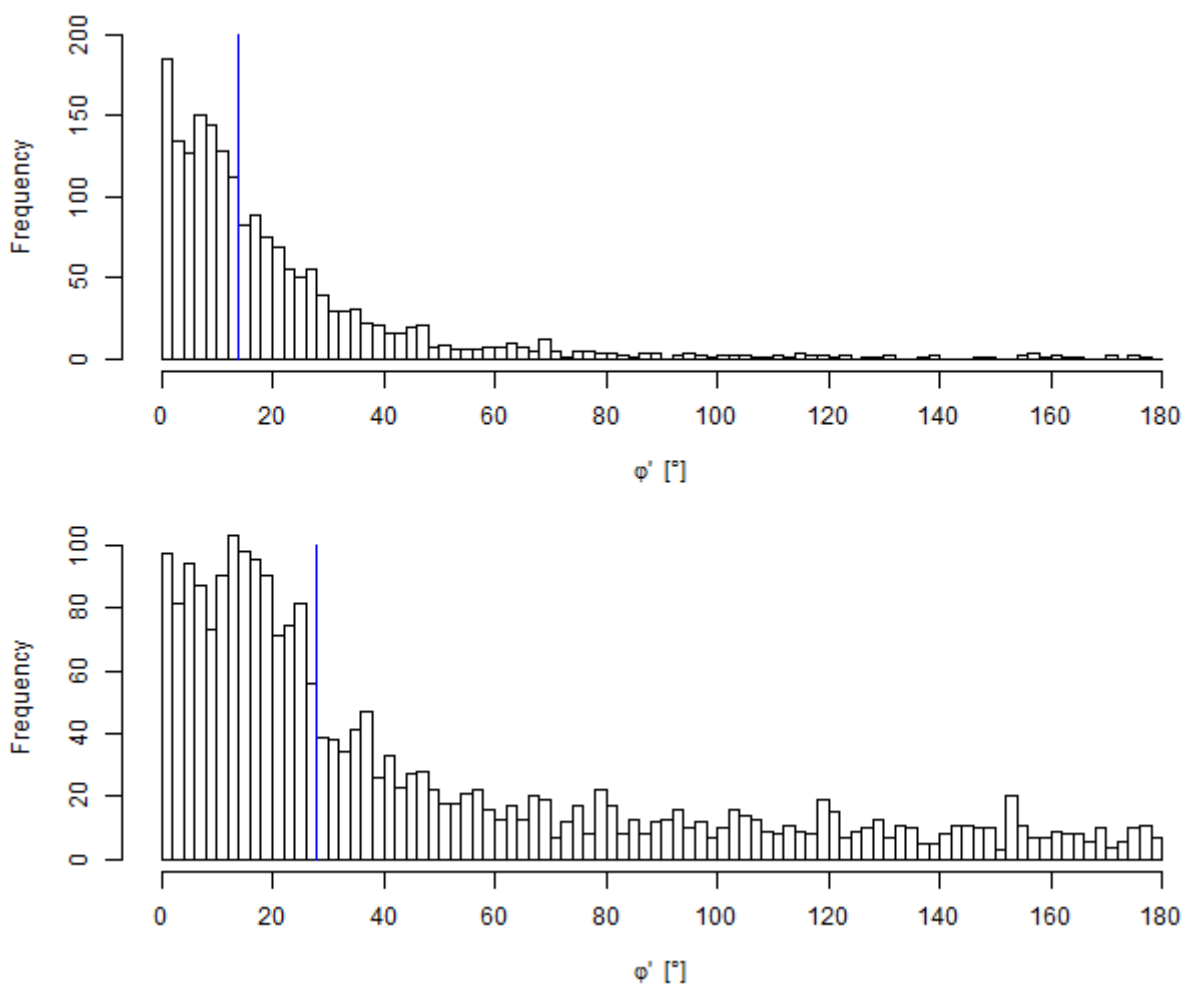


Figure 5: Histogram of differences of wind direction between 180 m agl and 60 m agl during the day (upper one) and during the night (lower one)

### Velocity at a height of 100 m agl

- Weak: horizontal wind speeds are  $\leq 3.1 \text{ ms}^{-1}$  during the day and  $\leq 2.5 \text{ ms}^{-1}$  during the night in more than twice as much cases as in the class “strong”.
- Strong: horizontal wind speeds are  $> 3.1 \text{ ms}^{-1}$  during the day and  $> 2.5 \text{ ms}^{-1}$  during the night in more than twice as much cases as in the class “weak”.
- Not differentiated (ND): none of the classes “weak” or “strong” is true.

For the limits between weak wind and strong wind, the differences between the wind directions at the time  $t$  and at the time  $t + 10 \text{ min}$  was calculated and plotted versus the wind speed at the time  $t$ . Furthermore, a regression line was fitted using the local polynomial regression fitting tool “loess” in R. The limits were set at points where the gradient of the loess-line (solid red line in Figure 6) differs visibly from the line with zero slope (dashed blue line in Figure 6).

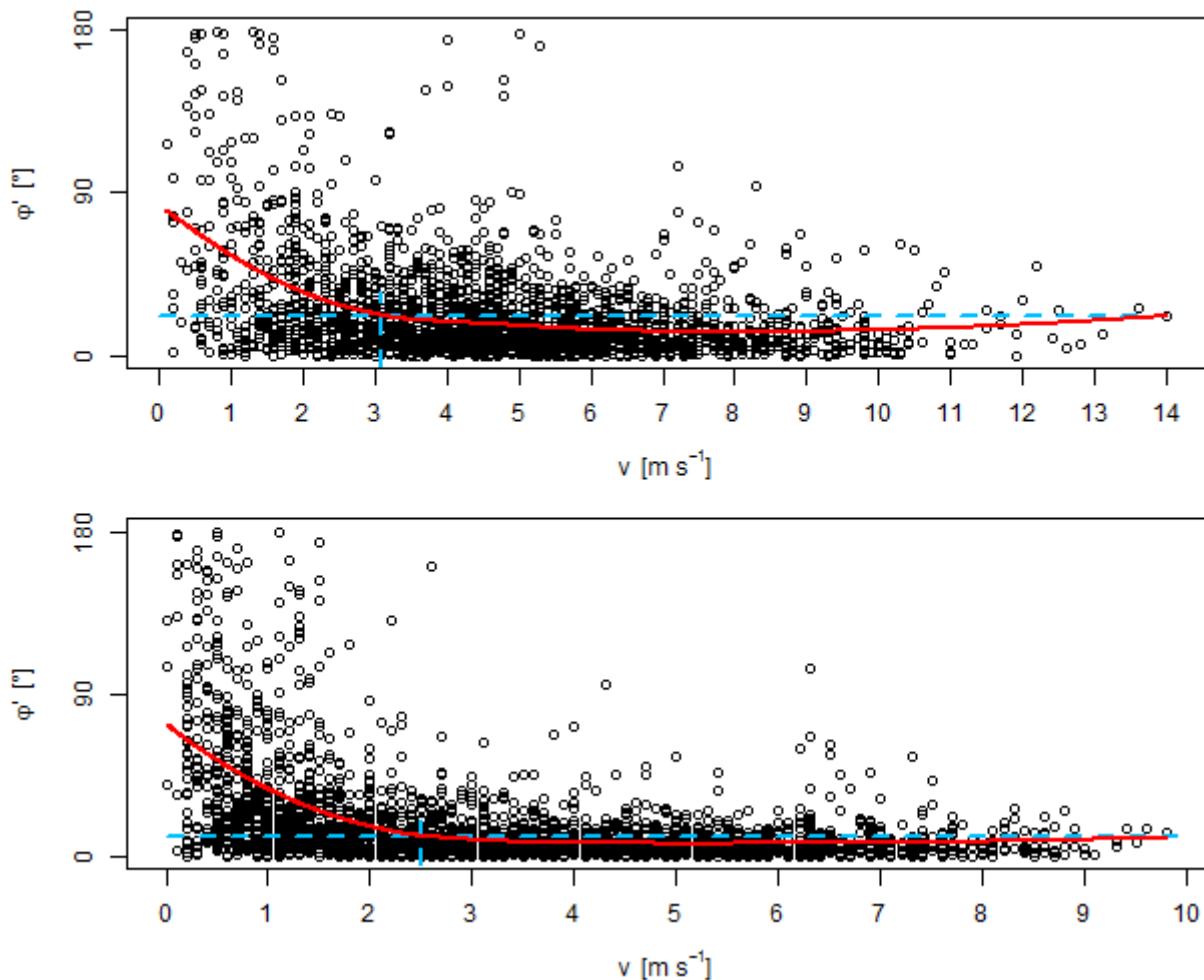


Figure 6: Difference of wind direction between  $t$  and  $t+10 \text{ min}$  versus wind speed at  $t$  at 100 m agl during the day (upper one) and during the night (lower one) and fitted loess-line (solid red line)

### Stratification: difference of potential temperature between 180 m agl and 40 m agl

- Unstable & Neutral: the difference of the potential temperature is  $\leq 1.3$  K during the day and  $\leq 0.5$  K during the night in more than twice as much cases as in the class “stable”.
- Stable: the difference of the potential temperature is  $> 1.3$  K during the day and  $> 0.5$  K during the night in more than twice as much cases as in the class “unstable & neutral”.
- Not differentiated (ND): none of the classes “unstable & neutral” or “stable” is true.

The limits were set at points where there was an apparent break in the Histogram of differences of temperature between 180 m agl and 40 m agl (see Figure 7).

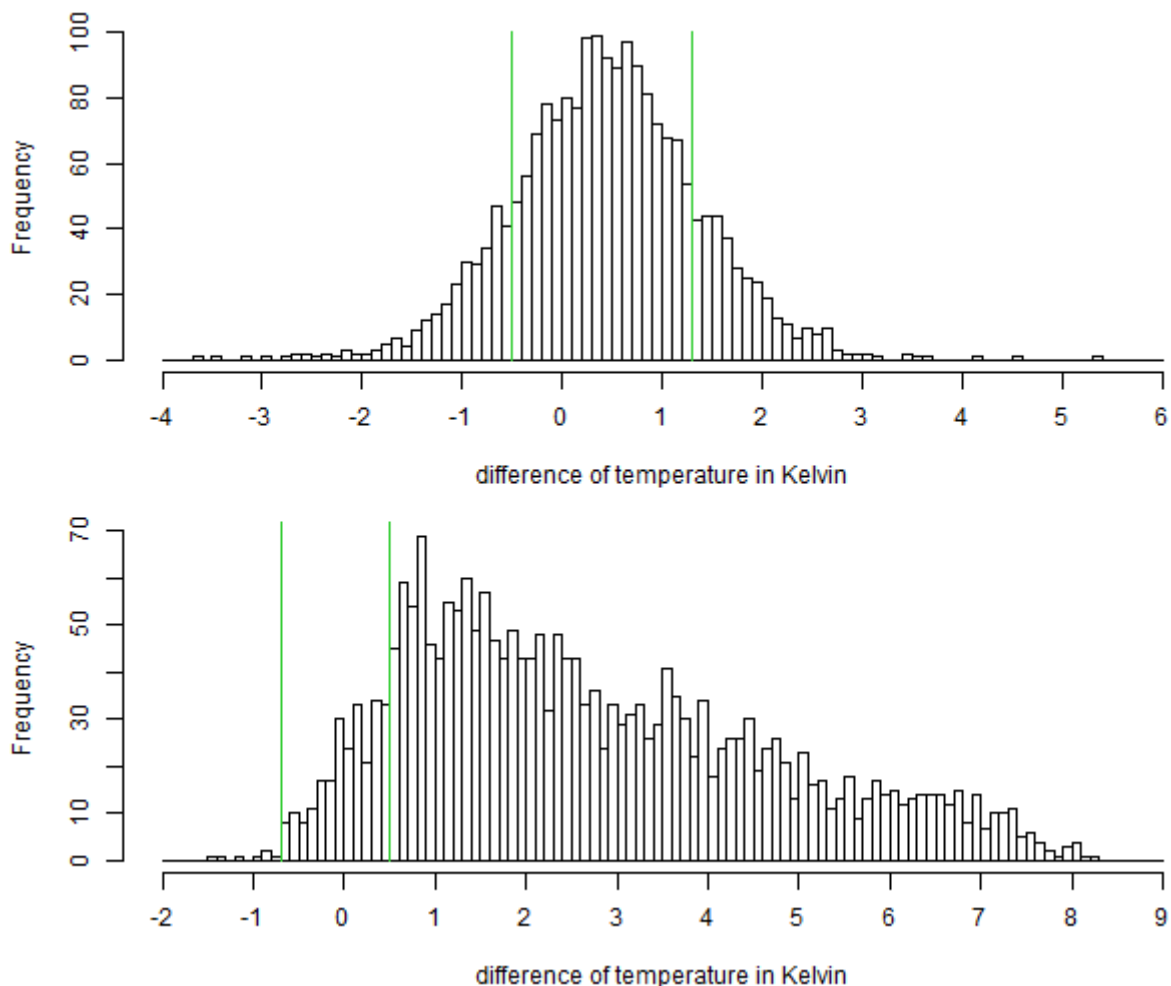
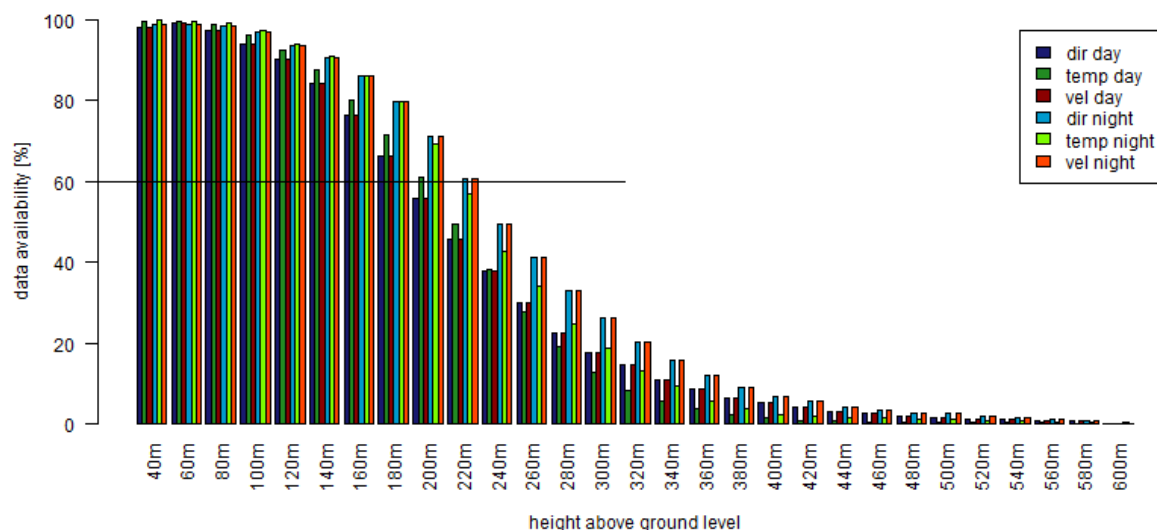


Figure 7: Histogram of differences of temperature between 180 m agl and 40 m agl during the day (upper one) and during the night (lower one)

The heights were chosen because of the distribution of the data availability (see Figure 8). At 100 m agl there is almost 100 % data availability, therefore 100 m agl was chosen as the reference height. For comparing two heights, 180 m agl was chosen as the upper height because there is more than 60 % data availability for every parameter. For the lower height, 40 m agl was chosen for the temperature to maximize the difference. For the wind direction, 60 m agl was chosen as the lower height.



**Figure 8: Data availability in percent for direction (dir), temperature (temp), and wind speed (vel) during the day and during the night**

Each class of one of the four criteria wind direction, difference of wind direction, velocity and stratification was combined with each of the other classes of the remaining three criteria. This resulted in 81 different cases, representing each combination that can be made. According to the class they fall in, each day and night was assigned to one of the 81 cases. This can be seen in Table 3 and Table 5 in appendix A. After assigning each day and night to a case, the number of days for each case was calculated. This distribution into the cases can be seen in Table 4 and Table 6 in appendix A. In Table 2 the distribution of days and nights can be seen. For analyzation and interpretation, only the cases were used where there were more than 2 days or nights. Furthermore, case 38 was analyzed and interpreted because it was the only case with wind direction “east” and case 71 was analyzed and interpreted because it had a very pronounced “difference of direction”. The values from the days or nights that fall in a case were averaged for every height and every time step if there were more than 2 values available. These ensemble averages were plotted with the program R and are displayed in the images for the different cases on the left-hand side. For the height profiles on the right-hand side, the

values from the days or nights that fall in a case were averaged for every height but not separated depending on the time. Here too, averages were only calculated, if there were more than 2 values available. Furthermore, the standard deviations were calculated for the height profiles.

**Table 2: Categories of selected Cases**

Case	Direction	Dif. of dir	Wind speed	Stratification	# of days	# of nights
6	West	ND	Strong	Neutral	18	0
4	West	Absent	Strong	Neutral	6	0
56	ND	Present	Weak	Neutral	3	0
5	West	Present	Strong	Neutral	2	0
63	ND	ND	ND	Neutral	2	0
13	West	Absent	Strong	Stable	0	6
15	West	ND	Strong	Stable	0	5
65	ND	Present	Weak	Stable	0	4
18	West	ND	ND	Stable	0	3
22	West	Absent	Strong	ND	1	3
38	East	Present	Weak	Stable	0	2
66	ND	ND	Weak	Stable	0	2
71	ND	Present	ND	Stable	0	2

For additional support for the evaluation of the images, the radiation data of a weather station was used. The weather station “Voitsumra” is run by the micrometeorology group of the University of Bayreuth in cooperation with the BayCEER (Bayreuth Center for Ecology and Environmental Research) and is located directly next the SODAR RASS. For case 6, 4 and 56, the global solar radiation and the balance of downwelling longwave radiation and surface radiation were ensemble averaged in the same way as the observations of the SODAR. For the cases that represent the nights, the counter radiation and the balance of counter radiation and surface radiation were averaged.

#### **4.2. Comparison of Station 2 and Station 1**

It was intended to compare the wind profile from Station 1 and Station 2. The height difference between Station 1 and Station 2 is 453 m (see Figure 10), so the upper 200 to 300 m of the observations at station 2 could have been compared to the measured values of Station 1. Unfortunately, the height range of the SODAR RASS at station 2 was not overlapping with that of the SODAR at station 1. That means that a comparison between the two stations was not possible. As can be seen in Figure 8, above 220 m agl, there is less than 50 % data

availability during the day. During the night, above 240 m agl, there is less than 50 % data availability.

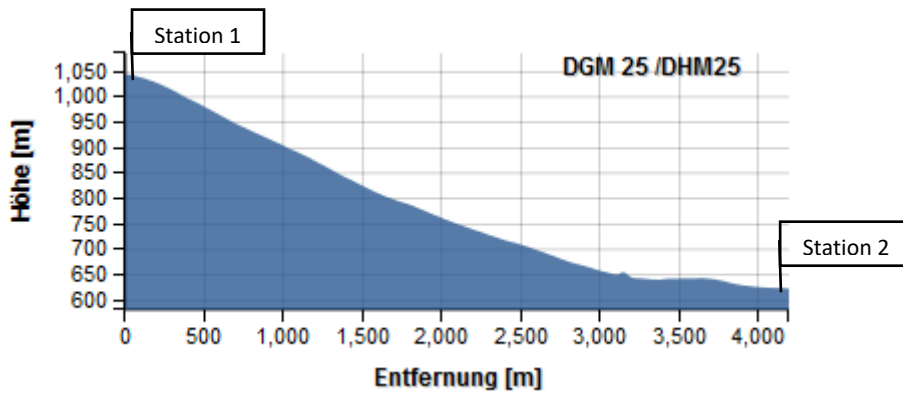


Figure 9: Height profile of the route Schneeberg (Station 1) – Voitsumra (Station 2)

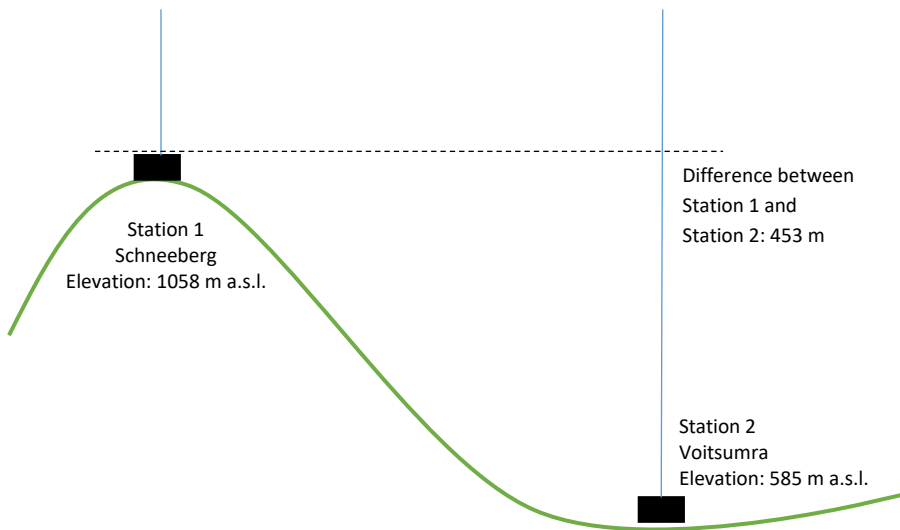


Figure 10: Height profile of the route Schneeberg (Station 1) – Voitsumra (Station 2) with height difference

## 5. Results

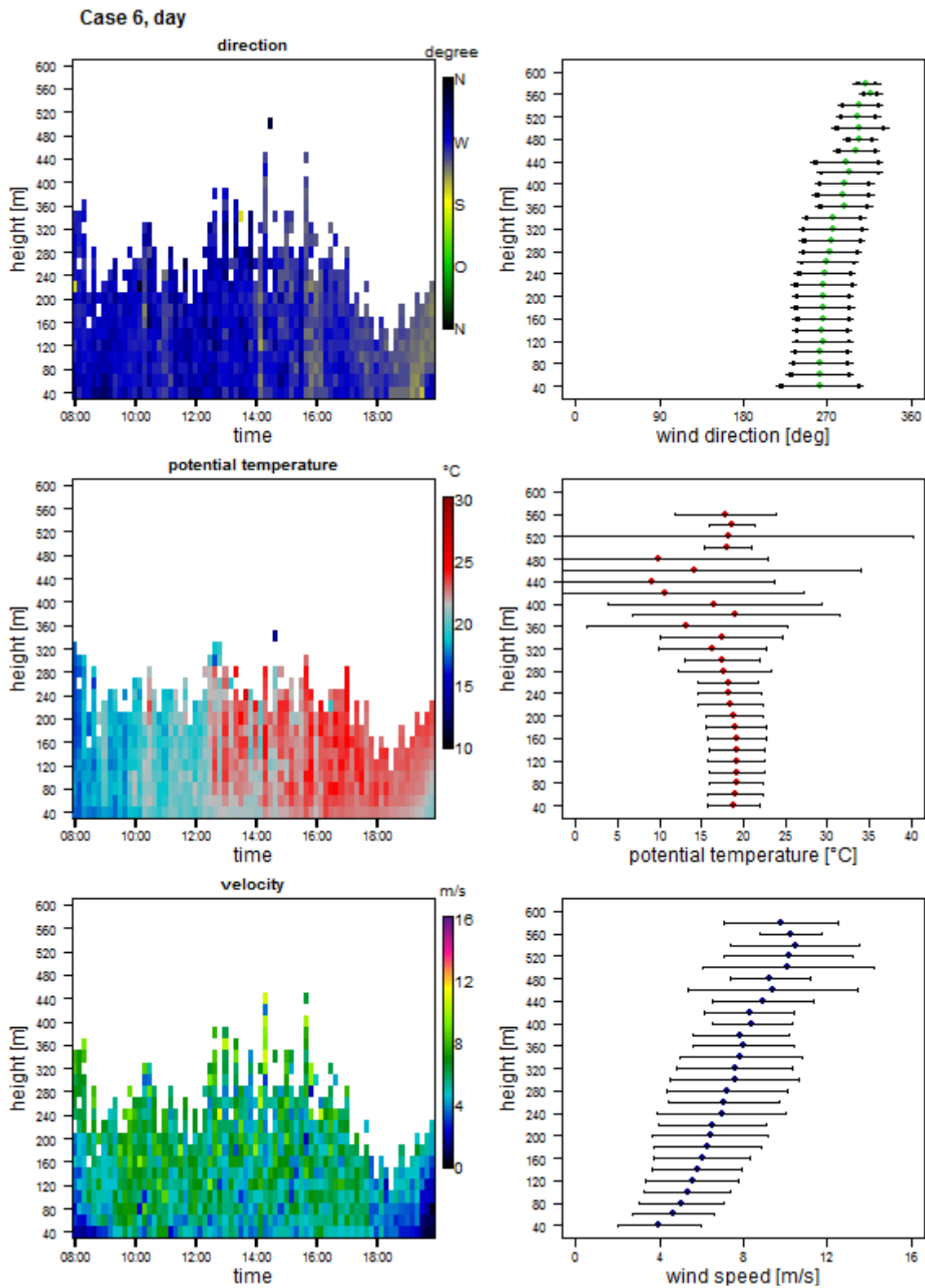


Figure 11: Case 6, part 1 (n = 18) – On the left: ensemble-averaged time-height plots, on the right: height profile with standard deviation

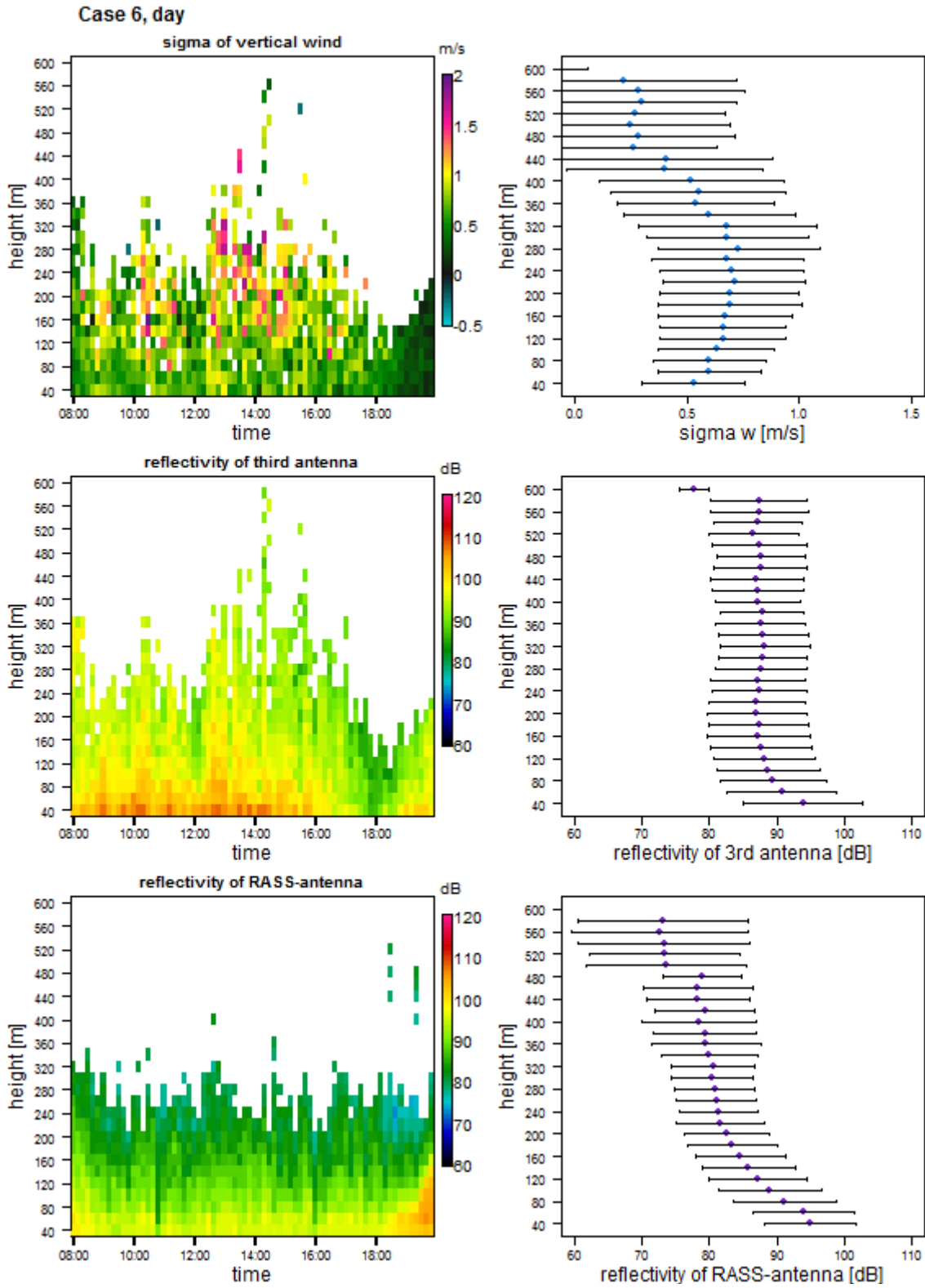


Figure 12: Case 6, part 2 (n = 18) – On the left: ensemble-averaged time-height plots, on the right: height profile with standard deviation

Case 6 was classified as: direction: west; difference of direction: not differentiated; wind speed: strong; stratification: neutral.

In this case, the wind is coming from the west with almost no change of the direction with the height and a low standard deviation. From the 40 days that are analyzed, 18 days from case 6 and 6 days from case 4 have “West” as the wind direction. Together that is 24 days with “West” as the wind direction. This indicates that West is the main wind direction, which makes sense, considering that Germany is located in the zone of the Westerlies of the middle latitudes (Malberg 2007).

The atmosphere is stratified neutral in the lowest 40 to 160 m agl and slightly unstable from a height of about 180 m agl to 320 m agl. This indicates a clear inversion layer in the lower 160 m agl. The potential temperature is about 18 °C at the ground and decreases to 16 °C in a height of 320 m agl. Above 320 m agl the standard deviation gets very high indicating greater differences in the temperature. It could also be due to the fact that there is very little data available at that height.

The wind speed is high with about 4 to 11 ms<sup>-1</sup>. It increases from 4 ms<sup>-1</sup> at 40 m height agl to about 11 ms<sup>-1</sup> in a height of 540 m agl. This is due to the friction at the ground which leads to an almost logarithmic wind profile.

The standard deviation of the vertical wind speed is relatively high due to great turbulence because of the high wind speed. The reflectivity of the third antenna decreases a little bit but then stays the same because of the great turbulence. The turbulence means that there are enough density inhomogeneities, where the sound waves can be reflected. The reflectivity of the RASS-antenna decreases more with height because of the increasing wind speeds. The sound waves that are needed for the scattering of the electromagnetic waves are carried away faster if the wind speeds are higher.

In Figure 13 the global solar radiation shows little spikes and the net longwave radiation, which is the downwelling longwave radiation minus the surface radiation, is relatively high and increasing during the day. This means that there was a relatively clear sky during the day.

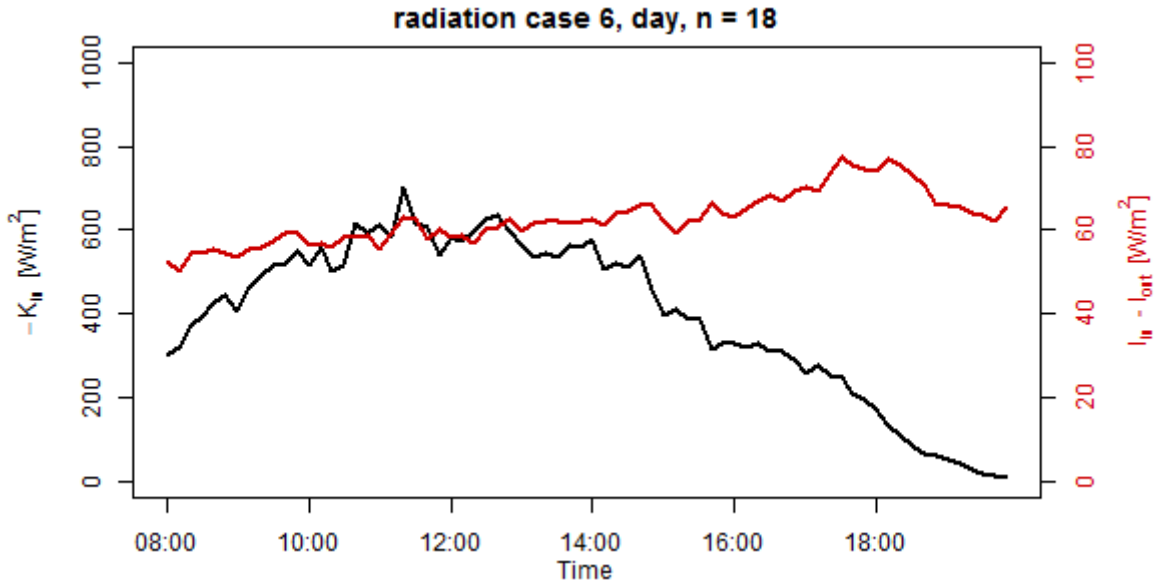


Figure 13: Case 6 – Global solar radiation ( $K_{in}$ ) and net longwave radiation ( $l_{in} - l_{out}$ )

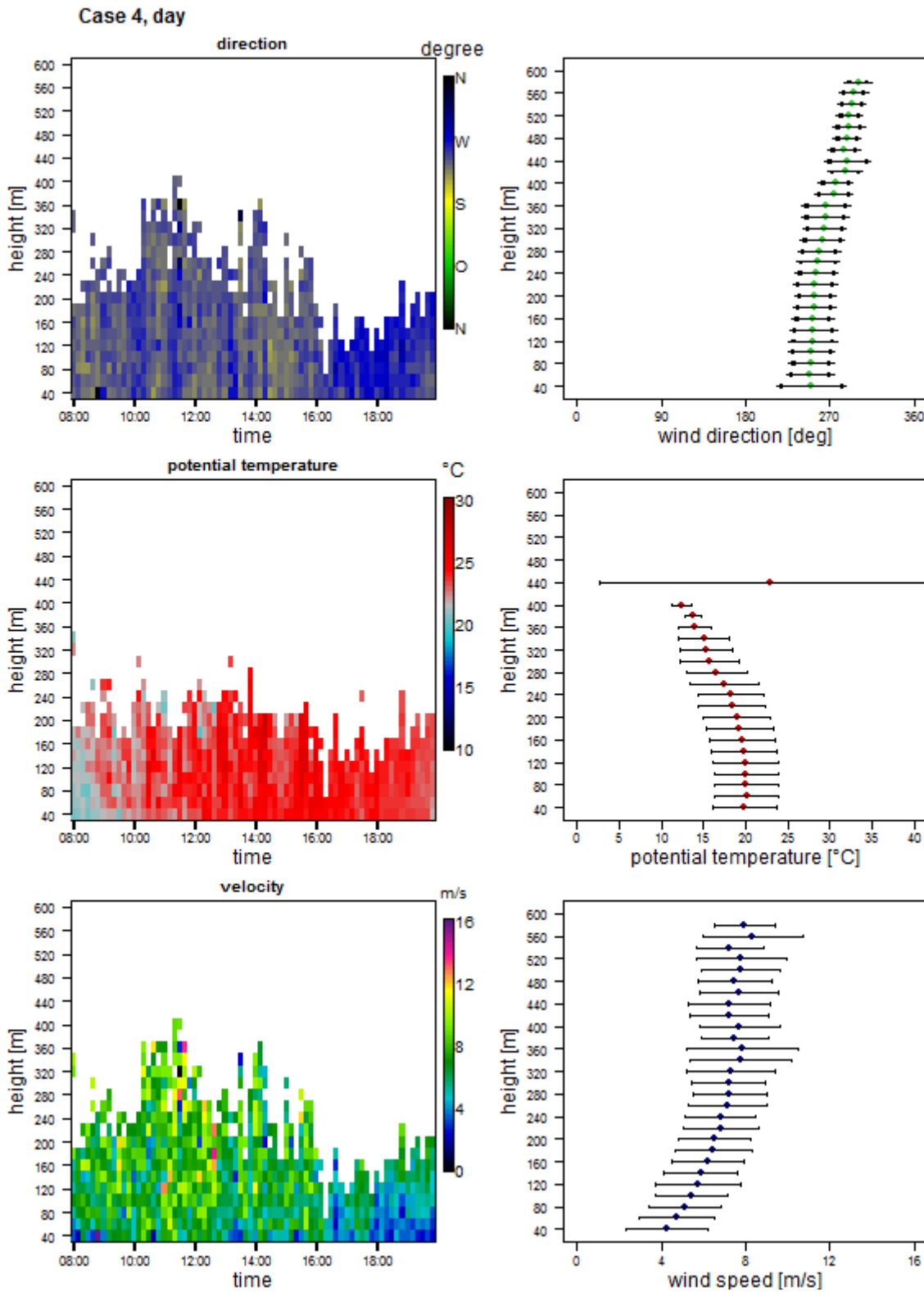


Figure 14: Case 4, part 1 (n = 6) – On the left: ensemble-averaged time-height plots, on the right: height profile with standard deviation

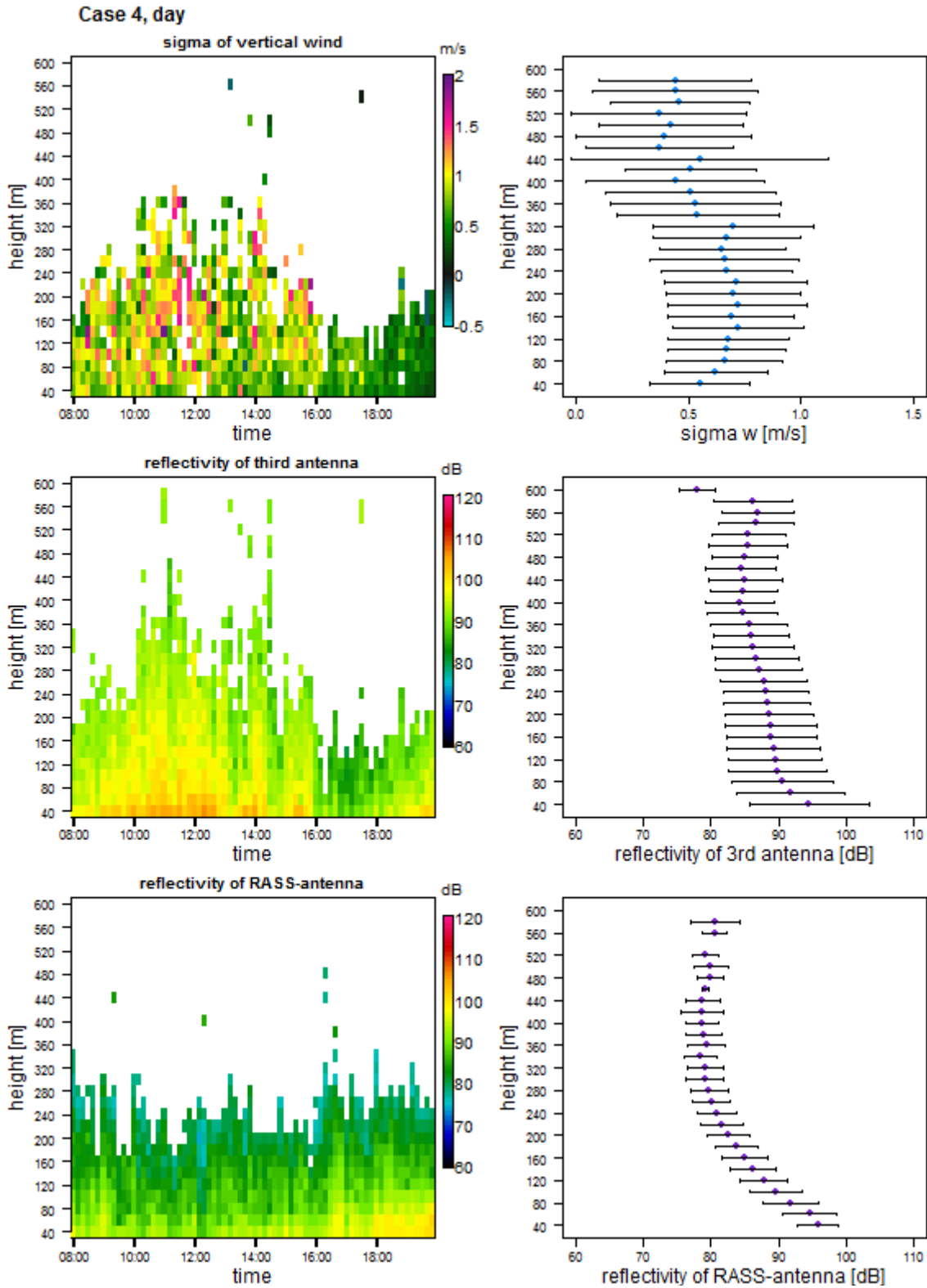


Figure 15: Case 4, part 2 (n = 6) – On the left: ensemble-averaged time-height plots, on the right: height profile with standard deviation

Case 4 was classified as: direction: west; difference of direction: absent; wind speed: strong; stratification: neutral.

Case 4 is similar to case 6, although there are some differences. The wind direction is West with a very small standard deviation. The stratification is neutral until 200 m height agl, above it gets unstable. This indicates a clear inversion layer in the lower 160 m. The potential temperature is a bit higher than in case 6, it is 20 °C at 40 m height agl and decreases to 12 °C at a height of 400 m agl. The wind speed is 4 ms<sup>-1</sup> at the bottom and increases to about 8 ms<sup>-1</sup> at a height of 340 m agl from where it stays almost the same. The sigma of the vertical wind is high in this case as well as there are high wind speeds. As in case 6, the reflectivity of the third antenna decreases with height, but it stays on a lower level than the reflectivity of the RASS-antenna.

The global solar radiation in Figure 16 is rather low and shows a lot of spikes. The net longwave radiation is lower than in Figure 13. This indicates an overcast sky.

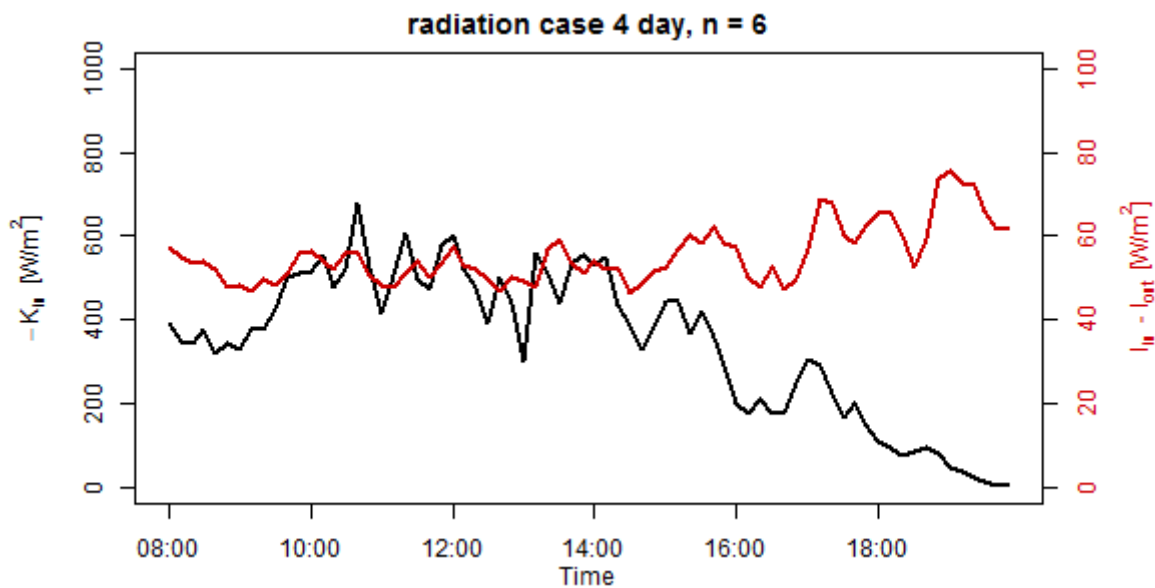


Figure 16: Case 4 – Global solar radiation ( $K_{in}$ ) and net longwave radiation ( $I_{in} - I_{out}$ )

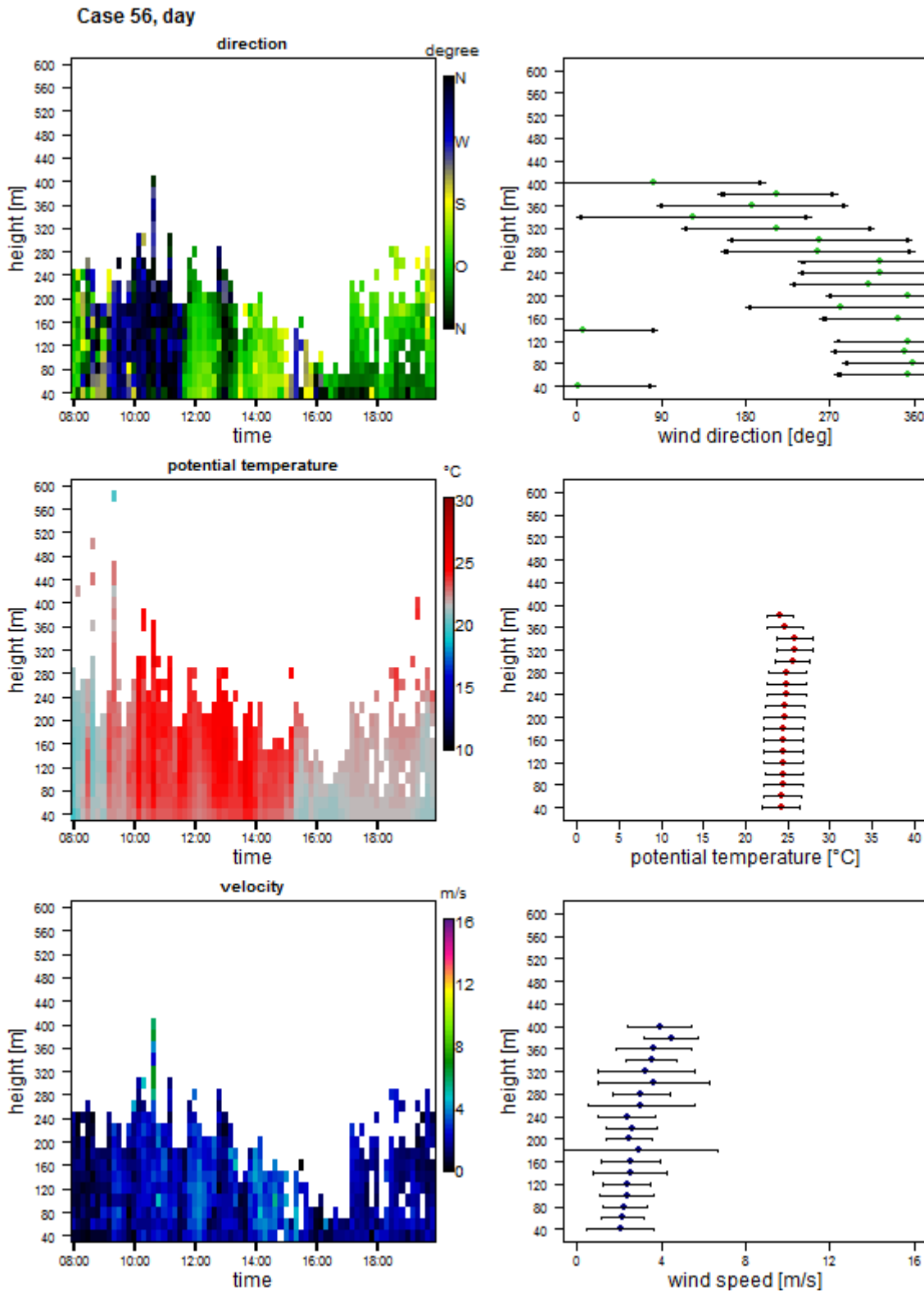


Figure 17: Case 56, part 1 (n = 3) – On the left: ensemble-averaged time-height plots, on the right: height profile with standard deviation

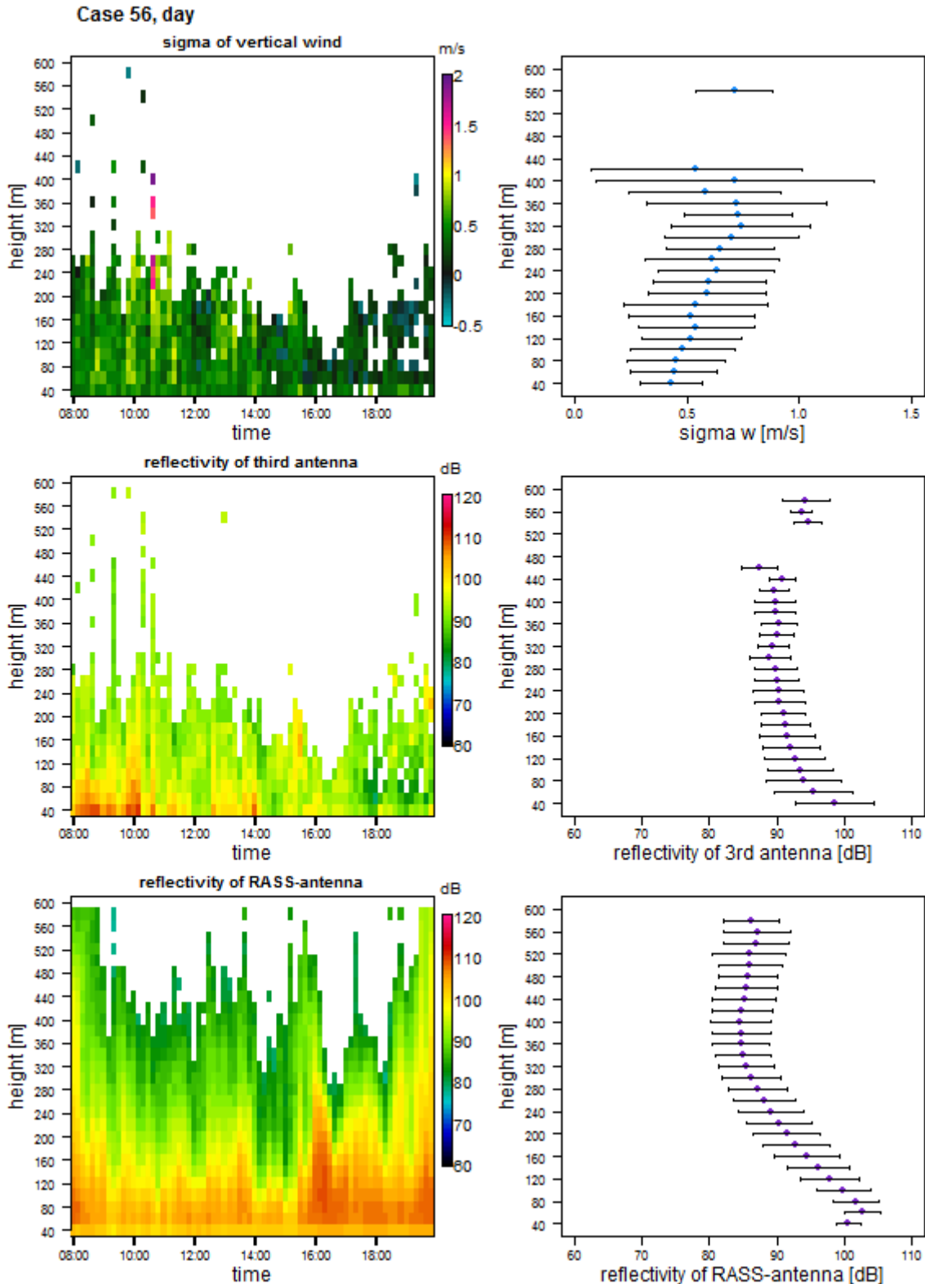


Figure 18: Case 56, part 2 (n = 3) – On the left: ensemble-averaged time-height plots, on the right: height profile with standard deviation

Case 56 was classified as: direction: not differentiated; difference of direction: present; wind speed: weak; stratification: neutral.

In this case the wind directions change notably over the day. In the height profile, the mean wind direction is changing from North at the ground to almost East at a height of 400 m agl with a high standard deviation. There are very low wind speeds of 2 to 4  $\text{ms}^{-1}$  and a low sigma of vertical wind which means little turbulence. Therefore the reflectivity of the RASS-antenna is very good. The atmosphere is slightly stable stratified, the temperatures increase from 23 to 26 °C.

The global solar radiation in Figure 19 shows a lot of spikes until 15:00. The net longwave radiation is relatively high, especially before 11:45 and after 15:00. That means, it was rather cloudy until 15:00, especially after 11:45. This corresponds to the temperatures, which are decreasing abruptly at 15:00 and to the wind direction, which is changing at 11:45.

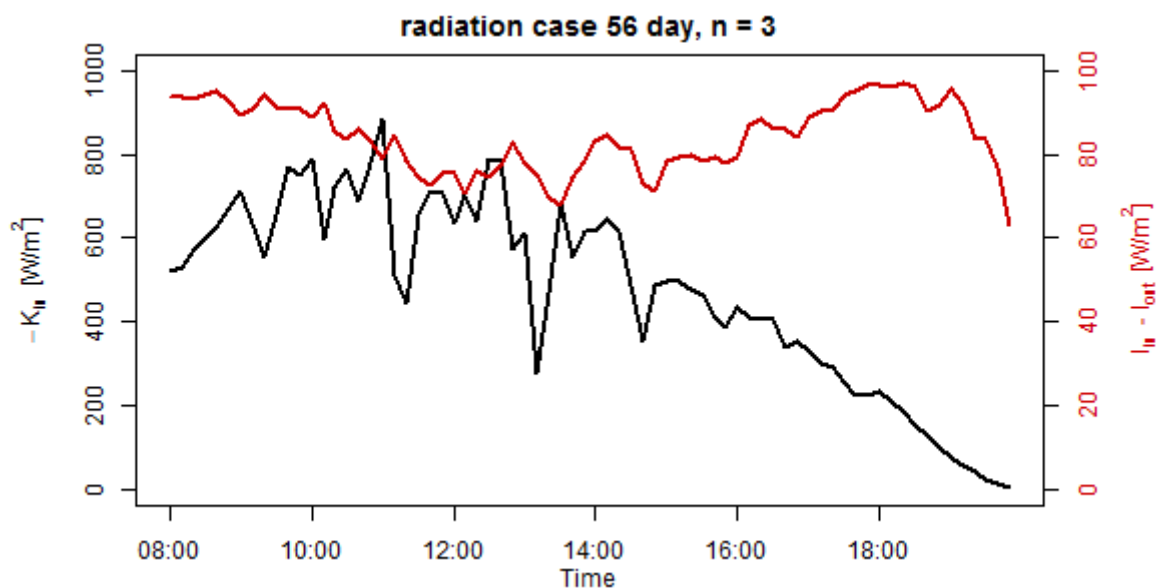


Figure 19: Case 56 – Global solar radiation ( $K_{in}$ ) and net longwave radiation ( $I_{in} - I_{out}$ )

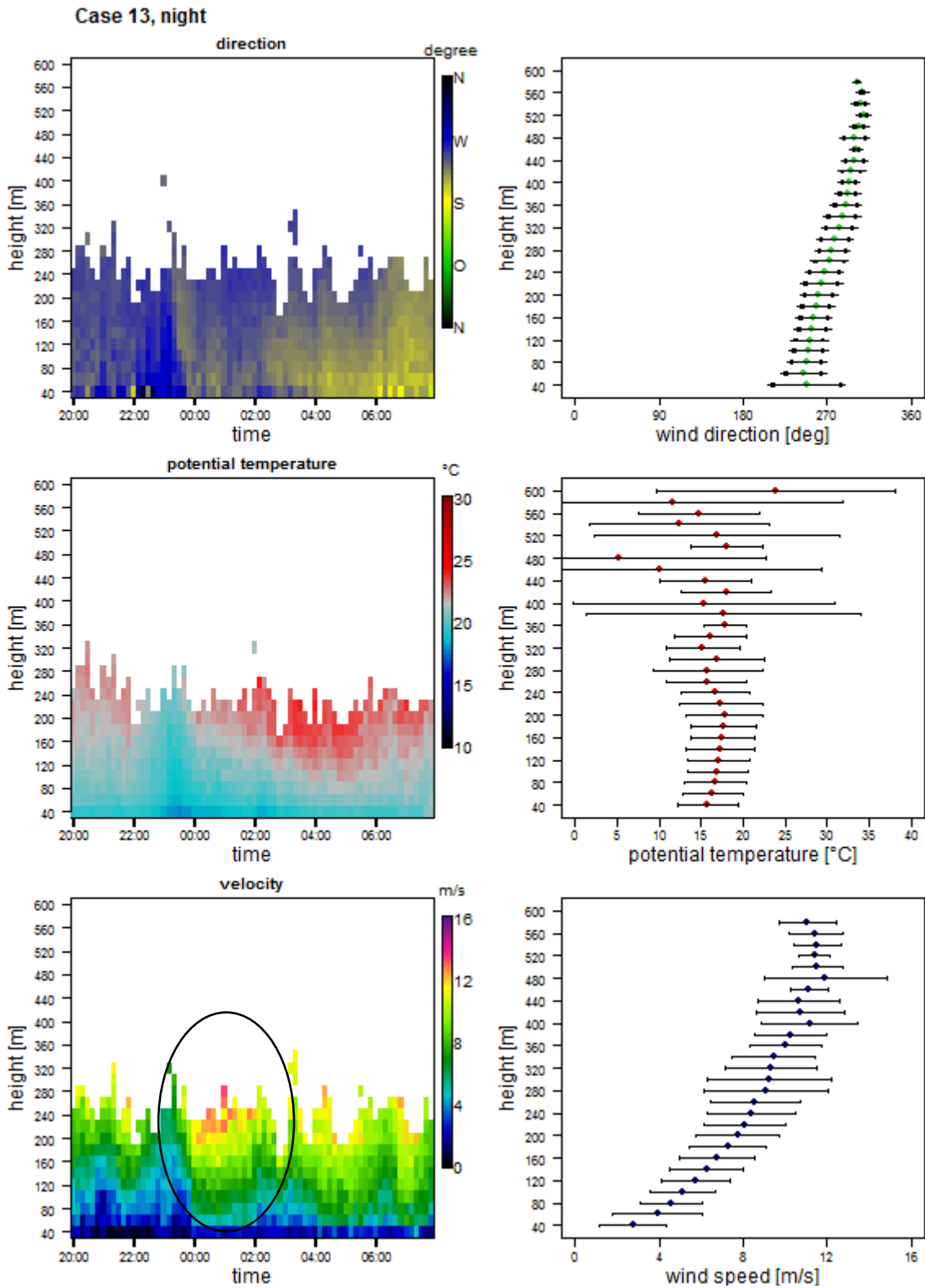


Figure 20: Case 13, part 1 (n = 6) – On the left: ensemble-averaged time-height plots, on the right: height profile with standard deviation

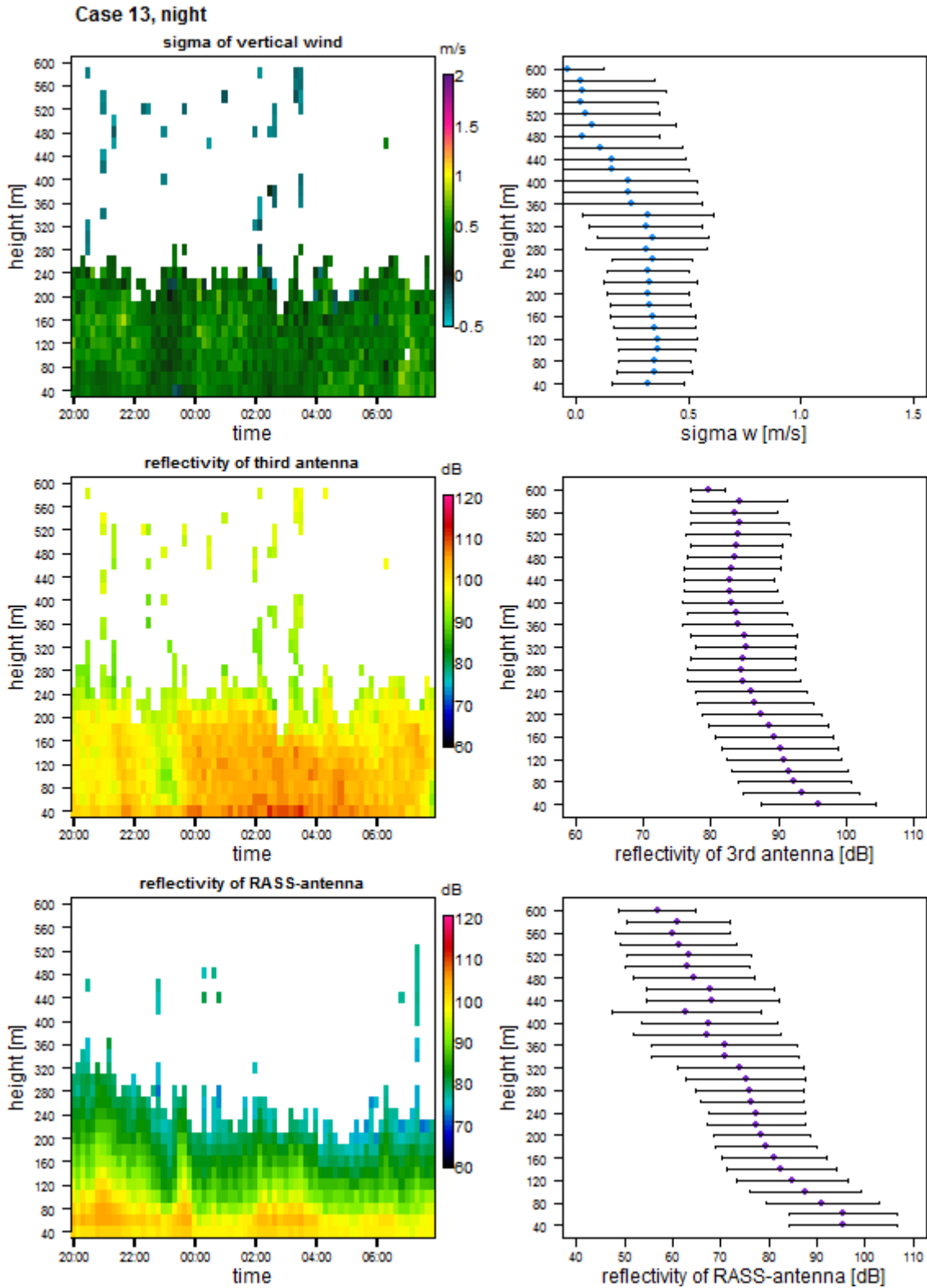


Figure 21: Case 13, part 2 (n = 6) – On the left: ensemble-averaged time-height plots, on the right: height profile with standard deviation

Case 13 was classified as: direction: west; difference of direction: absent; wind speed: strong; stratification: stable.

In case 13 there are west to south west winds with a very low standard deviation although there are 6 nights in this case. This means that the wind directions in these nights are all very similar. The wind speeds at the bottom are very low, about  $3 \text{ ms}^{-1}$ , increasing to  $12 \text{ ms}^{-1}$  at about 400 m height agl. This could be a low-level jet persisting over the whole night (marked with a circle in the ensemble-averaged time-height plot for the wind speed in Figure 20). The sigma of vertical wind is very low with only slightly increased sigma of vertical wind within areas of high wind speed due to the mechanically induced turbulence. The atmosphere is just slightly stable stratified with a lapse rate from  $2 \text{ }^{\circ}\text{C}$  in the lower 200 m, the temperature increasing from 15 to  $17 \text{ }^{\circ}\text{C}$ . Above, it gets unstable until 280 m agl. From 280 m agl upwards there is no gradient visible, maybe because of the small amount of available data in that height. The reflectivity of the third antenna decreases just slightly from 97 dB to 83 dB at a height of 580 m agl. The reflectivity of the RASS-antenna is falling more quickly from 97 dB to 56 dB at a height of 580 m agl.

In case 13, the downwelling longwave radiation is low and the net longwave radiation is high. This indicates a rather clear sky with little clouds during the night. This corresponds to the low temperatures.

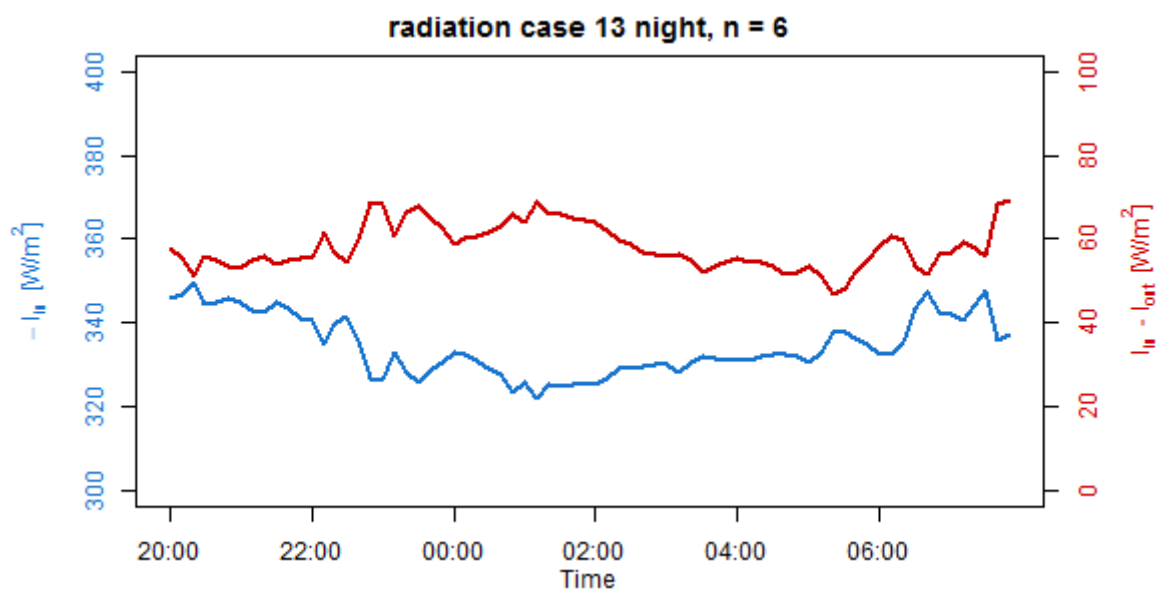


Figure 22: Case 13 – downwelling longwave radiation ( $l_{in}$ ) and net longwave radiation ( $l_{in} - l_{out}$ )

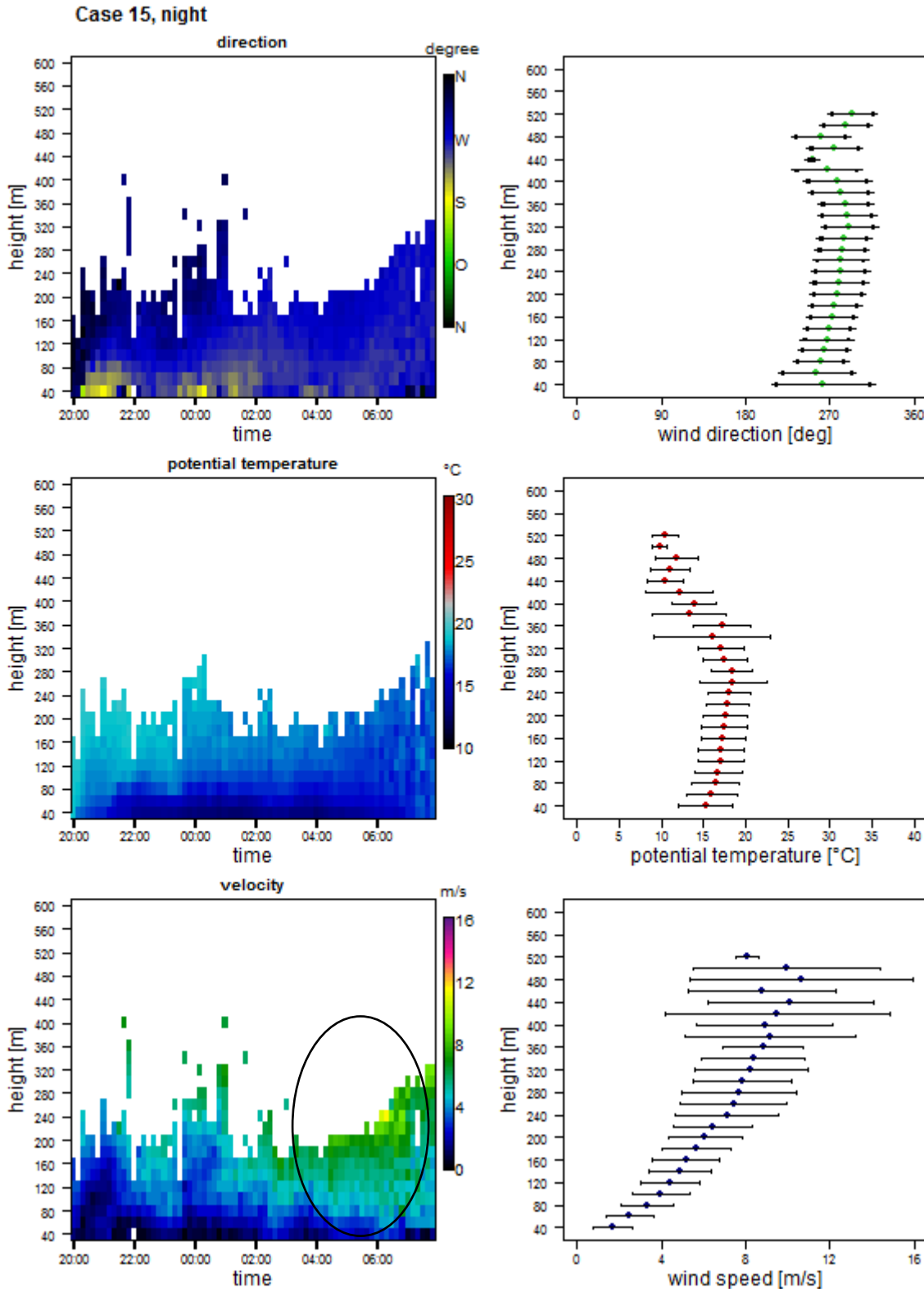


Figure 23: Case 15, part 1 (n = 5) – On the left: ensemble-averaged time-height plots, on the right: height profile with standard deviation

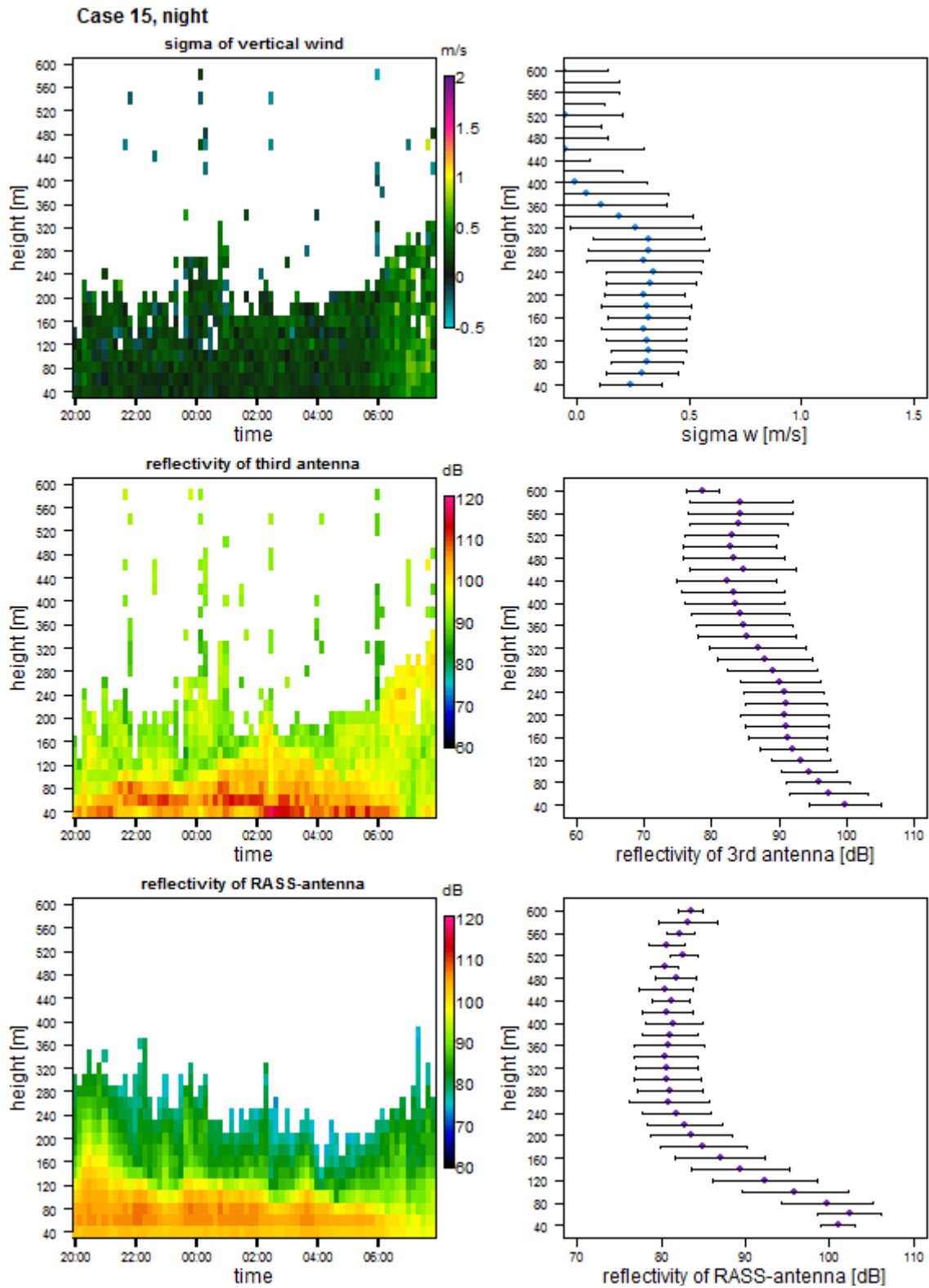


Figure 24: Case 15, part 2 ( $n = 5$ ) – On the left: ensemble-averaged time-height plots, on the right: height profile with standard deviation

Case 15 was classified as: direction: west; difference of direction: not differentiated; wind speed: strong; stratification: stable.

In case 15 the wind direction is West with a low standard deviation. The wind speeds at the bottom are very low, about  $2 \text{ ms}^{-1}$ , increasing to  $10 \text{ ms}^{-1}$  at about 500 m height agl. As in case 13, this could be a low-level jet persisting over the whole night, but weaker with lower wind speeds altogether (marked with a circle in the ensemble-averaged time-height plot for the wind speed in Figure 23). The sigma of vertical wind is very low. The stratification is stable with a lapse rate of 3 K in the lower 280 m. The temperatures increase from 15 to 18 °C. Above, the stratification gets unstable, the temperature decreases to 11 °C at a height of 520 m agl. This indicates an inversion layer in the lower 280 m.

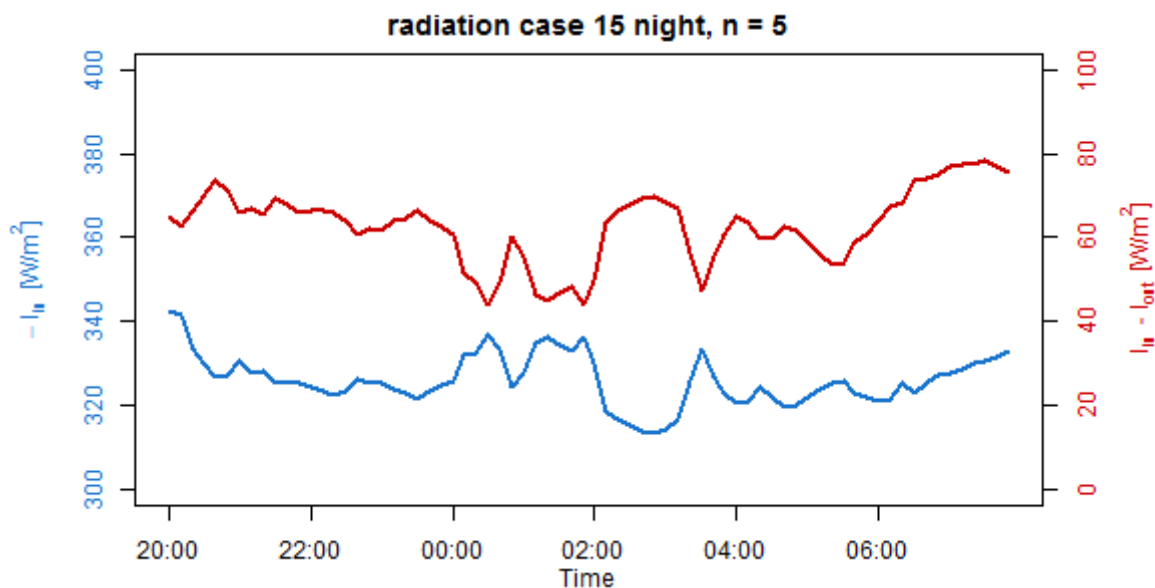


Figure 25: Case 15 – downwelling longwave radiation ( $l_{in}$ ) and net longwave radiation ( $l_{in} - l_{out}$ )

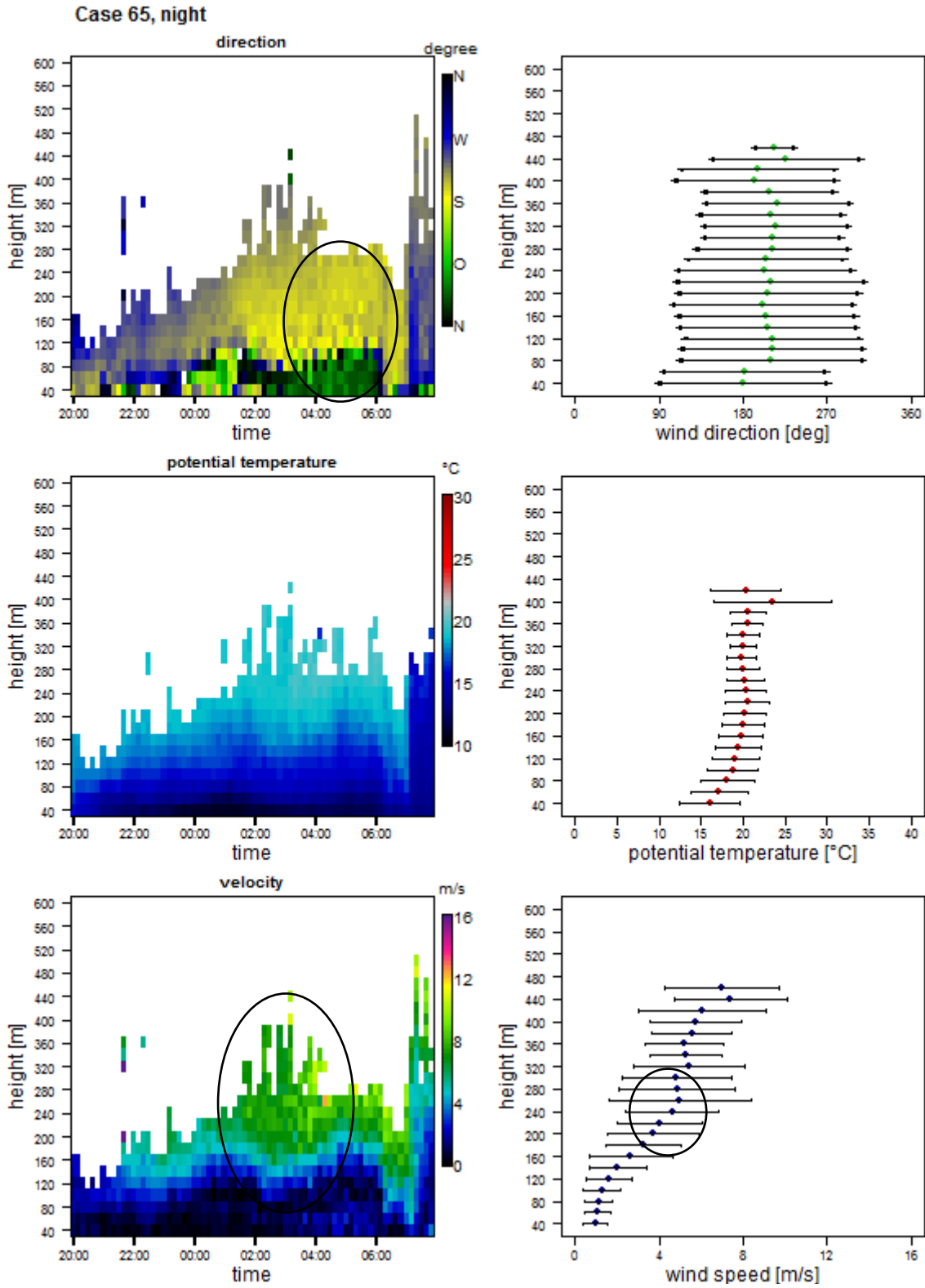


Figure 26: Case 65, part 1 (n = 4) – On the left: ensemble-averaged time-height plots, on the right: height profile with standard deviation

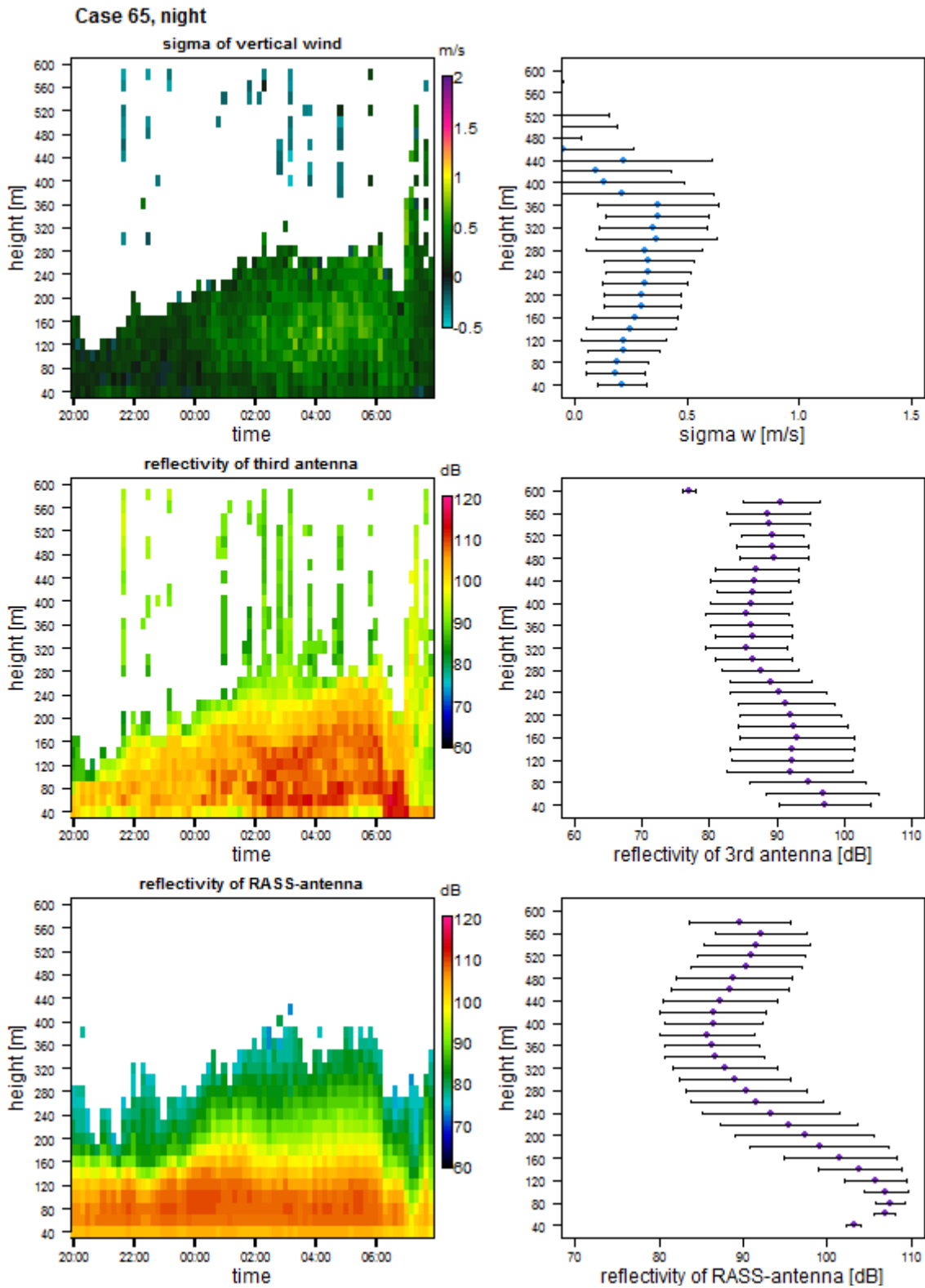


Figure 27: Case 65, part 2 (n = 4) – On the left: ensemble-averaged time-height plots, on the right: height profile with standard deviation

Case 65 was classified as: direction: not differentiated; difference of direction: present; wind speed: weak; stratification: stable.

In case 65 there is a distinct difference in the wind direction from  $180^\circ$  at 60 m height agl to  $210^\circ$  at 80 m height agl in the height profile. In the ensemble-averaged time-height plot it seems like a greater change from east to south west wind (marked with a circle in the ensemble-averaged time-height plot for the wind direction in Figure 26). This divergence might come from the averaging over the whole night. The sudden transition at a height of about 80 m agl is also visible in the wind speed. It is very low ( $1 \text{ ms}^{-1}$ ) until 80 m agl, above it is increasing until  $7 \text{ ms}^{-1}$  at a height of 460 m agl with a distinct bend at 220 m agl, where the stratification changes from stable to neutral (marked with a circle in the height profile for the wind speed in Figure 26). This indicates a relatively weak low-level jet (marked with a circle in the ensemble-averaged time-height plot for the wind speed in Figure 26). There is a higher sigma of vertical wind beneath areas of high wind speeds, maybe because of the low-level jet above causing turbulence beneath or lee vortices because the wind comes from the Schneeberg. The stratification is stable with  $16^\circ\text{C}$  at the bottom and  $20^\circ\text{C}$  at a height of 220 m agl. Above 220 m agl the stratification gets neutral.

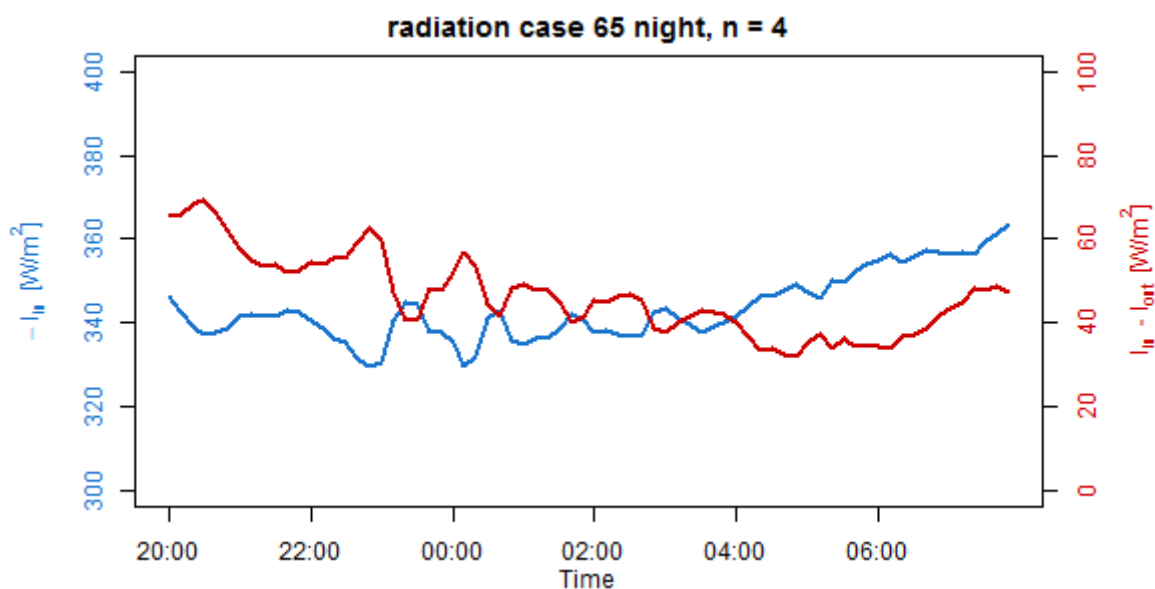


Figure 28: Case 65 – downwelling longwave radiation ( $I_{in}$ ) and net longwave radiation ( $I_{in} - I_{out}$ )

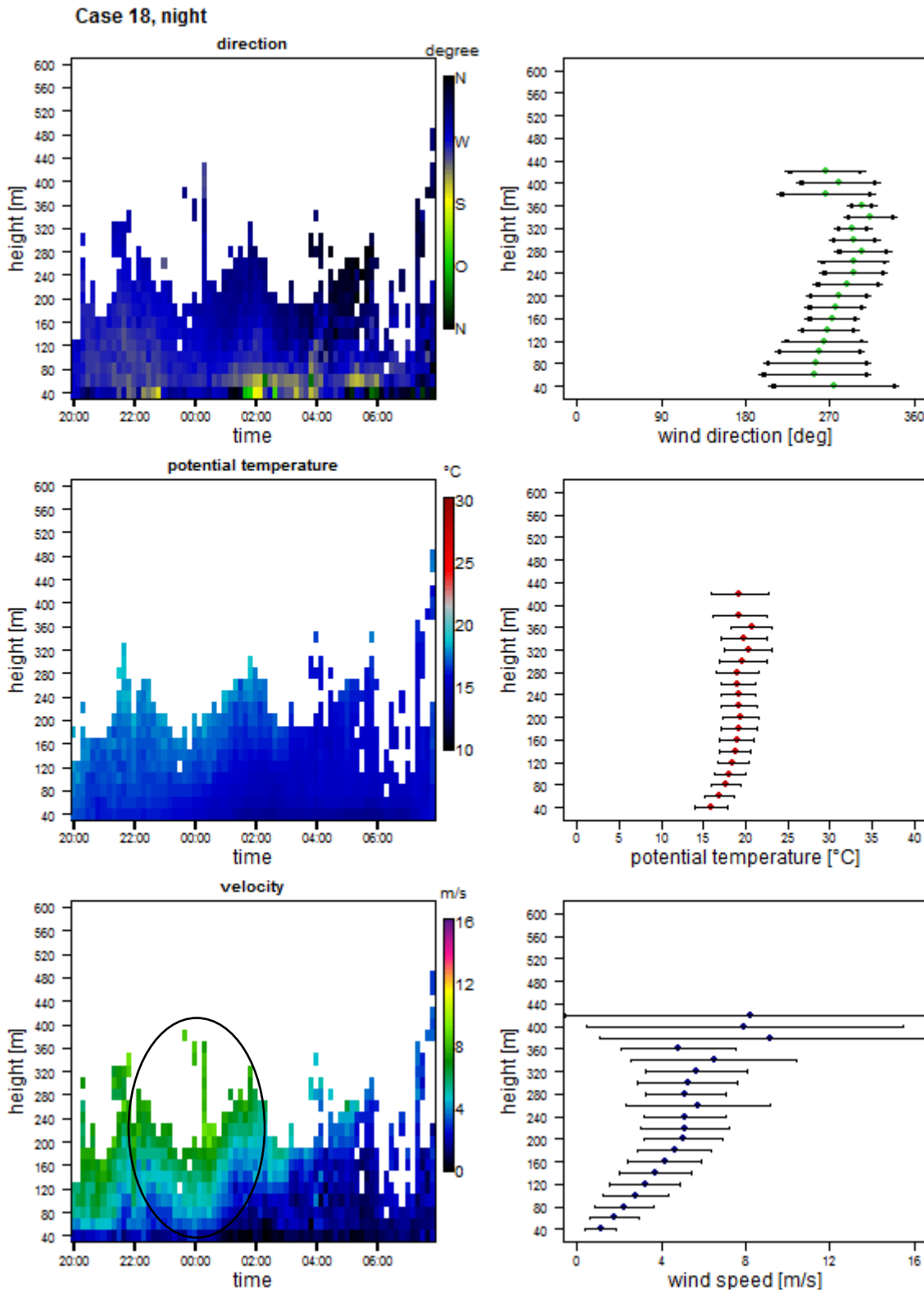


Figure 29: Case 18, part 1 (n = 3) – On the left: ensemble-averaged time-height plots, on the right: height profile with standard deviation

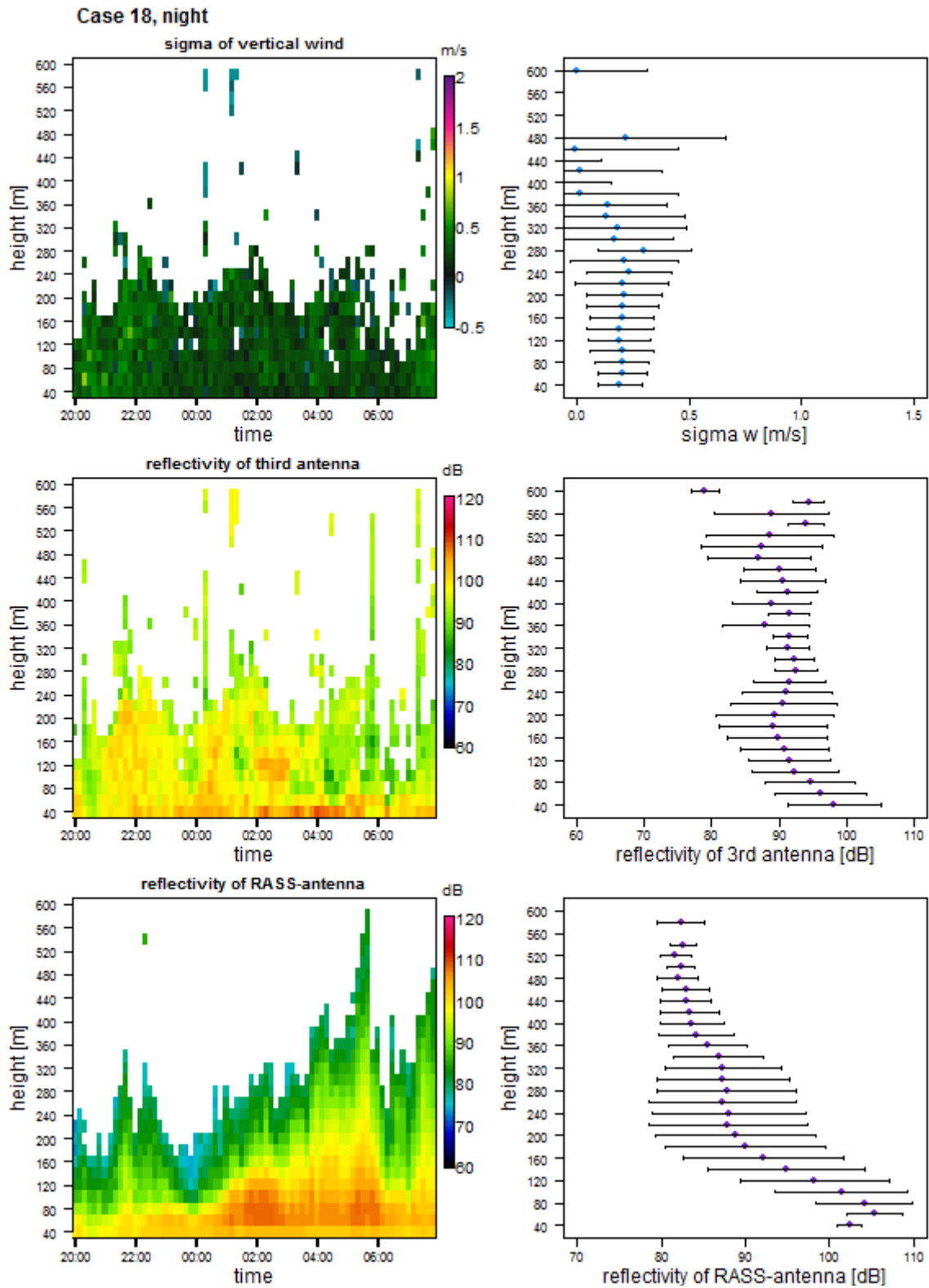


Figure 30: Case 18, part 2 ( $n = 3$ ) – On the left: ensemble-averaged time-height plots, on the right: height profile with standard deviation

Case 18 was classified as: direction: west; difference of direction: not differentiated; wind speed: not differentiated; stratification: stable.

In case 18, the wind direction is West with a relatively small standard deviation. In the ensemble-averaged time-height plot of the wind direction it looks like the wind is sometimes coming from the south. The wind speed is low ( $1 \text{ ms}^{-1}$ ) at the bottom and increases to  $8 \text{ ms}^{-1}$  at a height of 420 m agl. There is a visible bend in the wind speed at 200 m agl, which is also the height where the stratification shifts from stable to neutral. This bend is also visible in the reflectivity of the third antenna and the RASS-antenna. The reflectivity decreases strongly until this point and then stays almost the same (third antenna) or decreases slightly (RASS-antenna).

The counter radiation decreases strongly until about 02:00, while the net longwave balance increases. This indicates dissipating clouds and a clear sky from 00:00 to about 04:00. Then it gets cloudy again. This is related to the low-level jet, which is clearly visible in the first half of the night and then ceases (marked with a circle in the ensemble-averaged time-height plot for the wind speed in Figure 29).

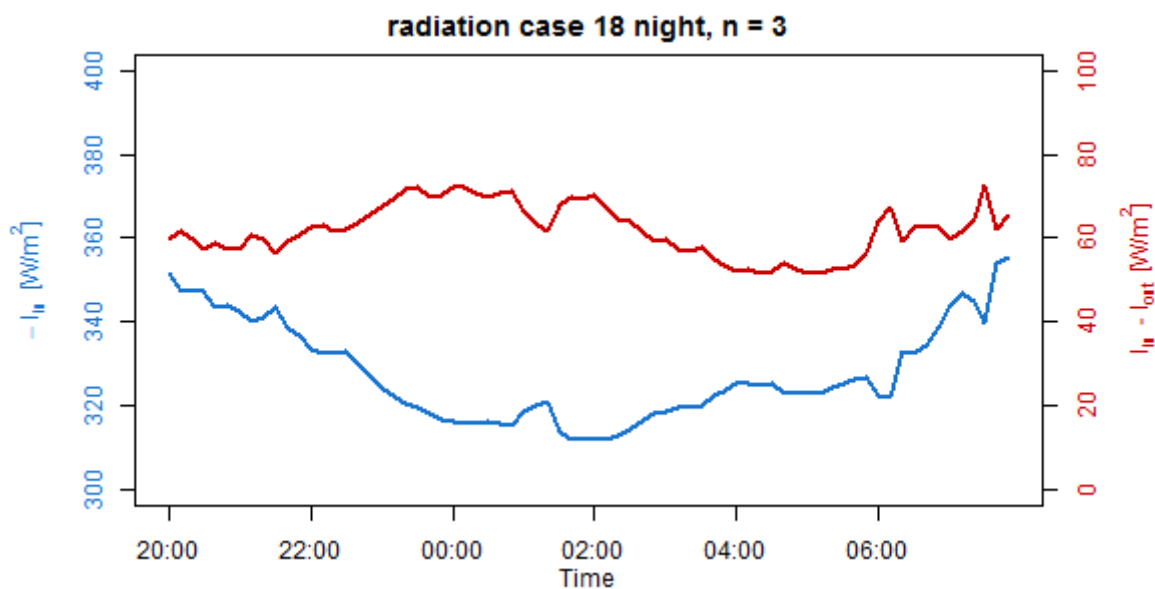


Figure 31: Case 18 – downwelling longwave radiation ( $I_{in}$ ) and net longwave radiation ( $I_{in} - I_{out}$ )

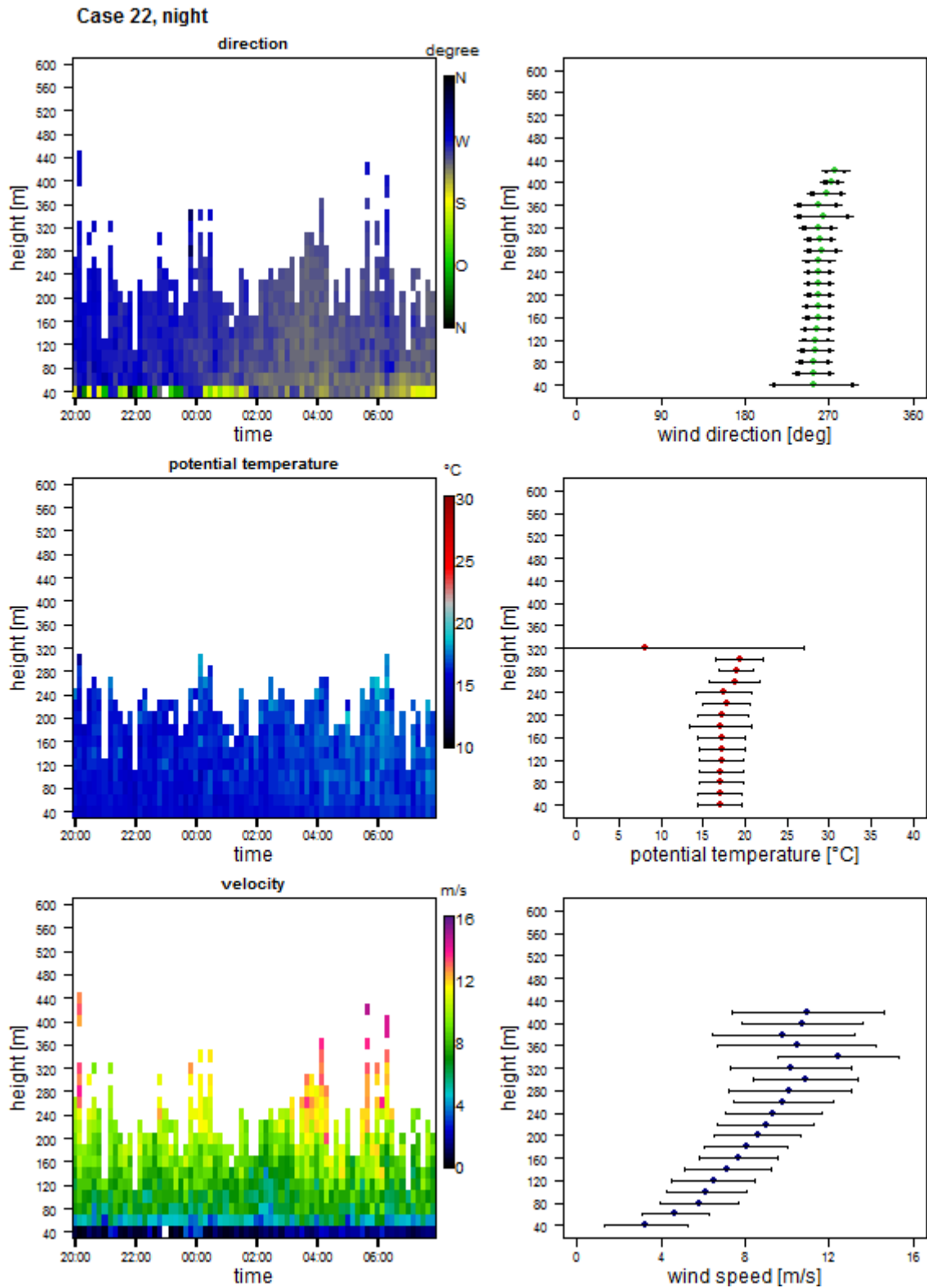


Figure 32: Case 22, part 1 ( $n = 3$ ) – On the left: ensemble-averaged time-height plots, on the right: height profile with standard deviation

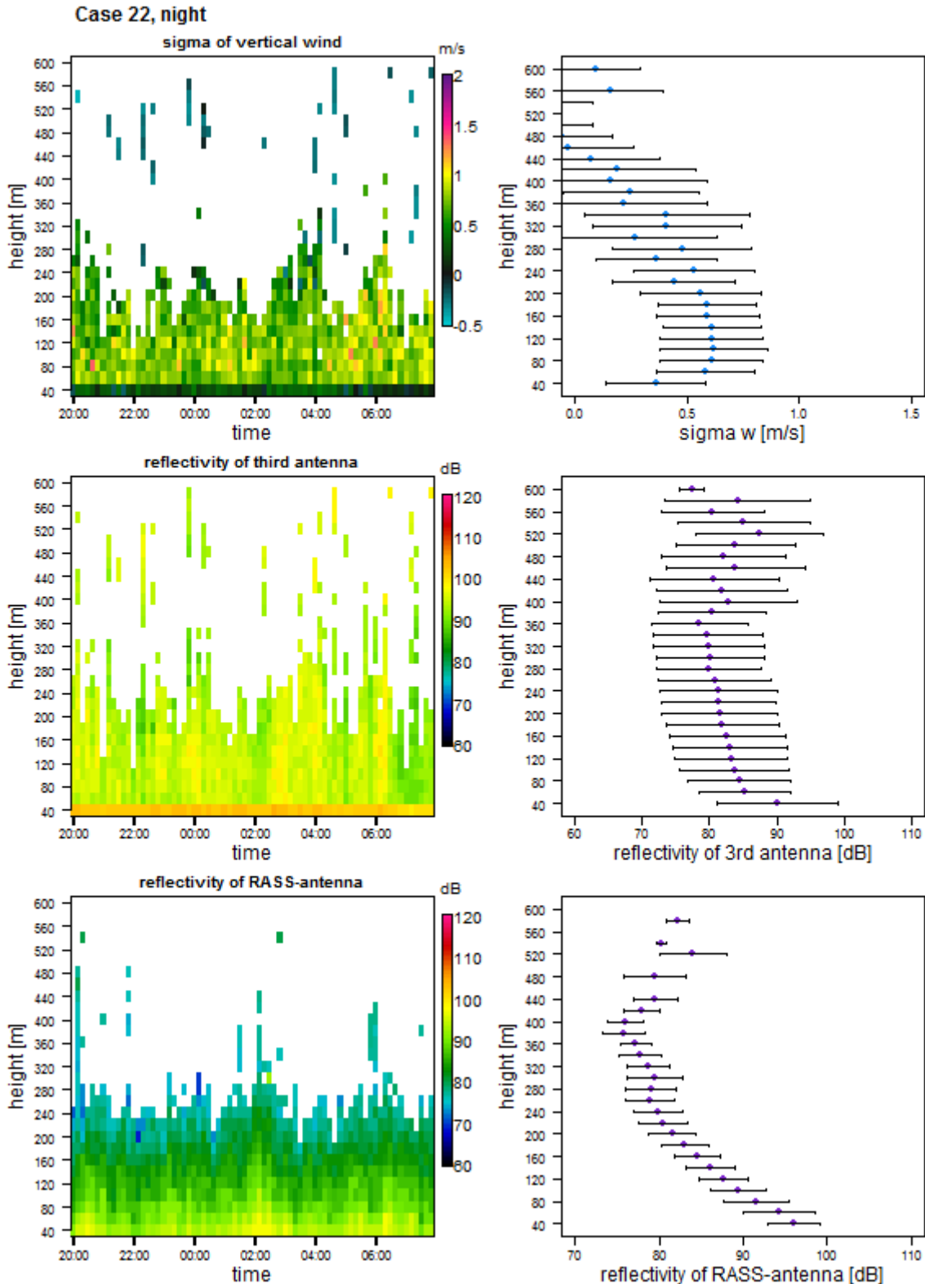


Figure 33: Case 22, part 2 (n = 3) – On the left: ensemble-averaged time-height plots, on the right: height profile with standard deviation

Case 22 was classified as: direction: west; difference of direction: absent; wind speed: strong; stratification: not differentiated.

In case 22 the wind direction is South-southwest with a very small standard deviation. There is a strong mesoscale wind, increasing very quickly from  $1 \text{ ms}^{-1}$  at the bottom to 10 to  $12 \text{ ms}^{-1}$  at about 300 m height agl. The sigma of vertical wind is high, due to strong mechanical shearing, therefore there is a lot of turbulence. The atmosphere is almost neutral stratified at  $17^\circ\text{C}$  with very uniform temperatures throughout the whole day and over the whole height profile. The reflectivity of the RASS-antenna decreases quickly from 97 dB at the bottom to 75 dB at a height of 400 m agl whereas the reflectivity of the third antenna stays on a higher level of about 82 dB.

In case 22, the net longwave radiation is rather low, while the counter radiation is high. This means the sky is overcast during the night, which corresponds to the strong mesoscale forcing.

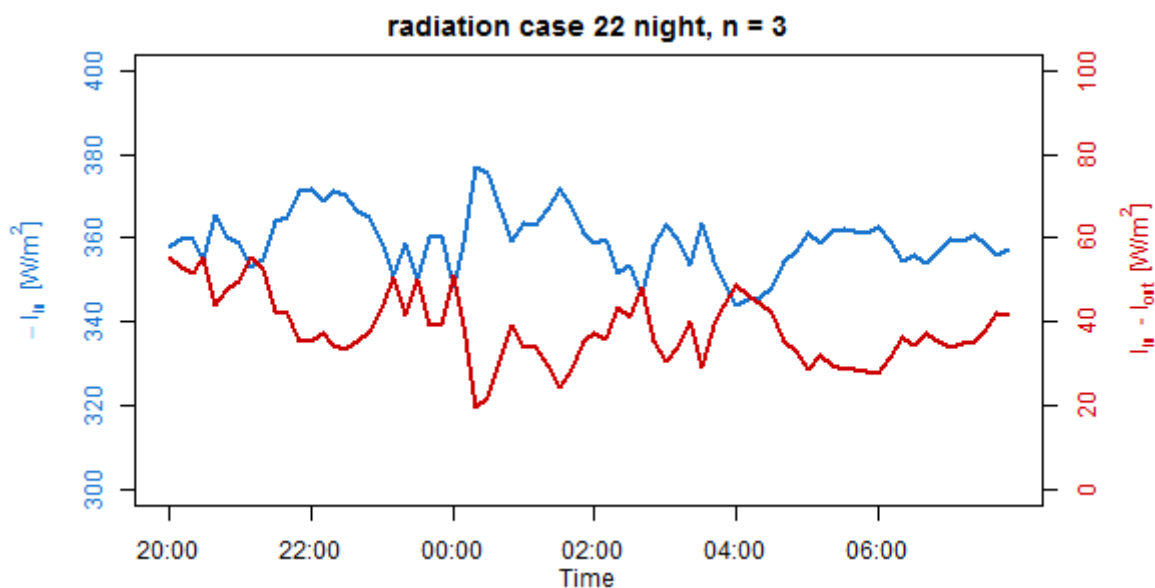


Figure 34: Case 22 – downwelling longwave radiation ( $I_{in}$ ) and net longwave radiation ( $I_{in} - I_{out}$ )

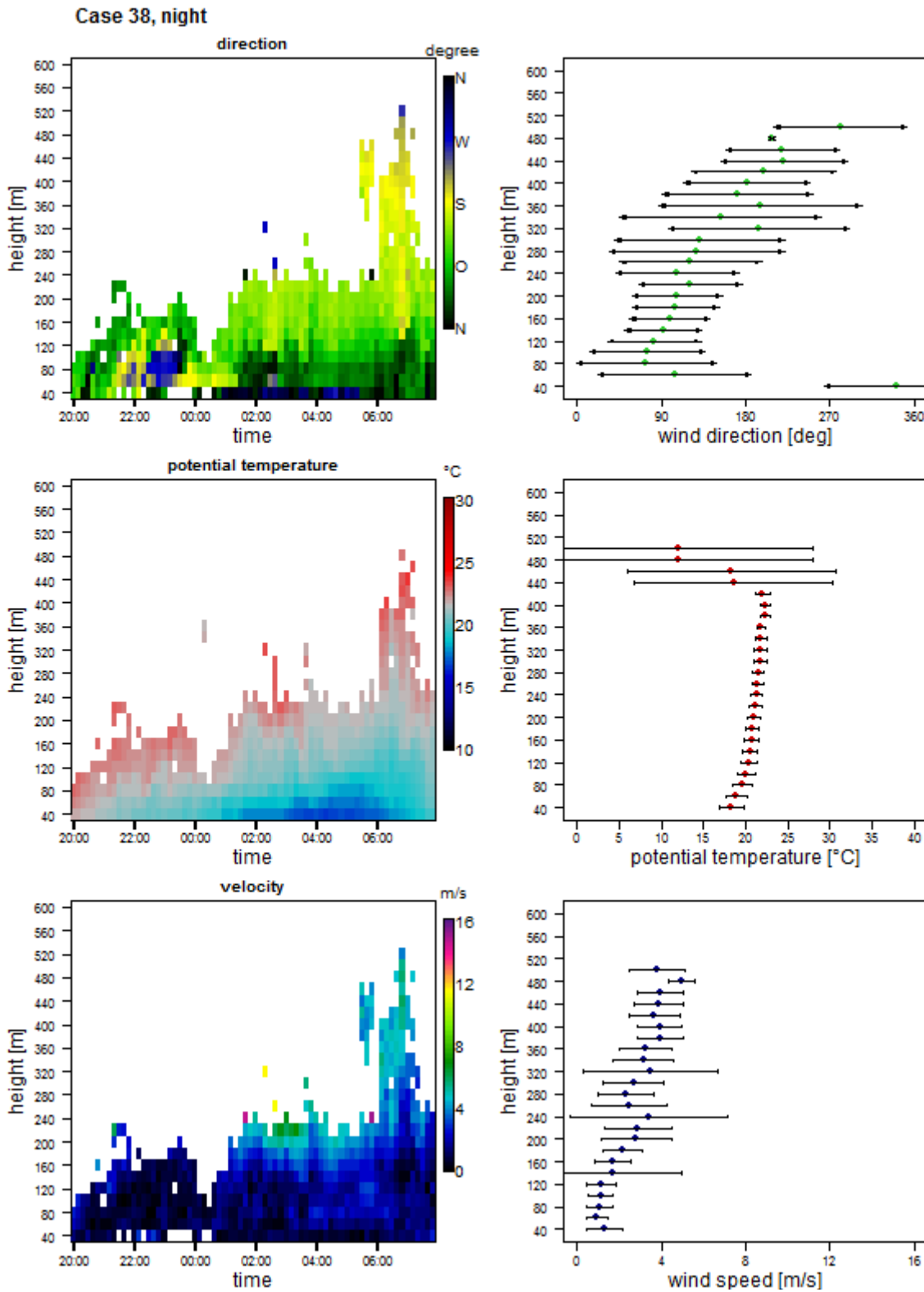


Figure 35: Case 38, part 1 (n = 2) – On the left: ensemble-averaged time-height plots, on the right: height profile with standard deviation

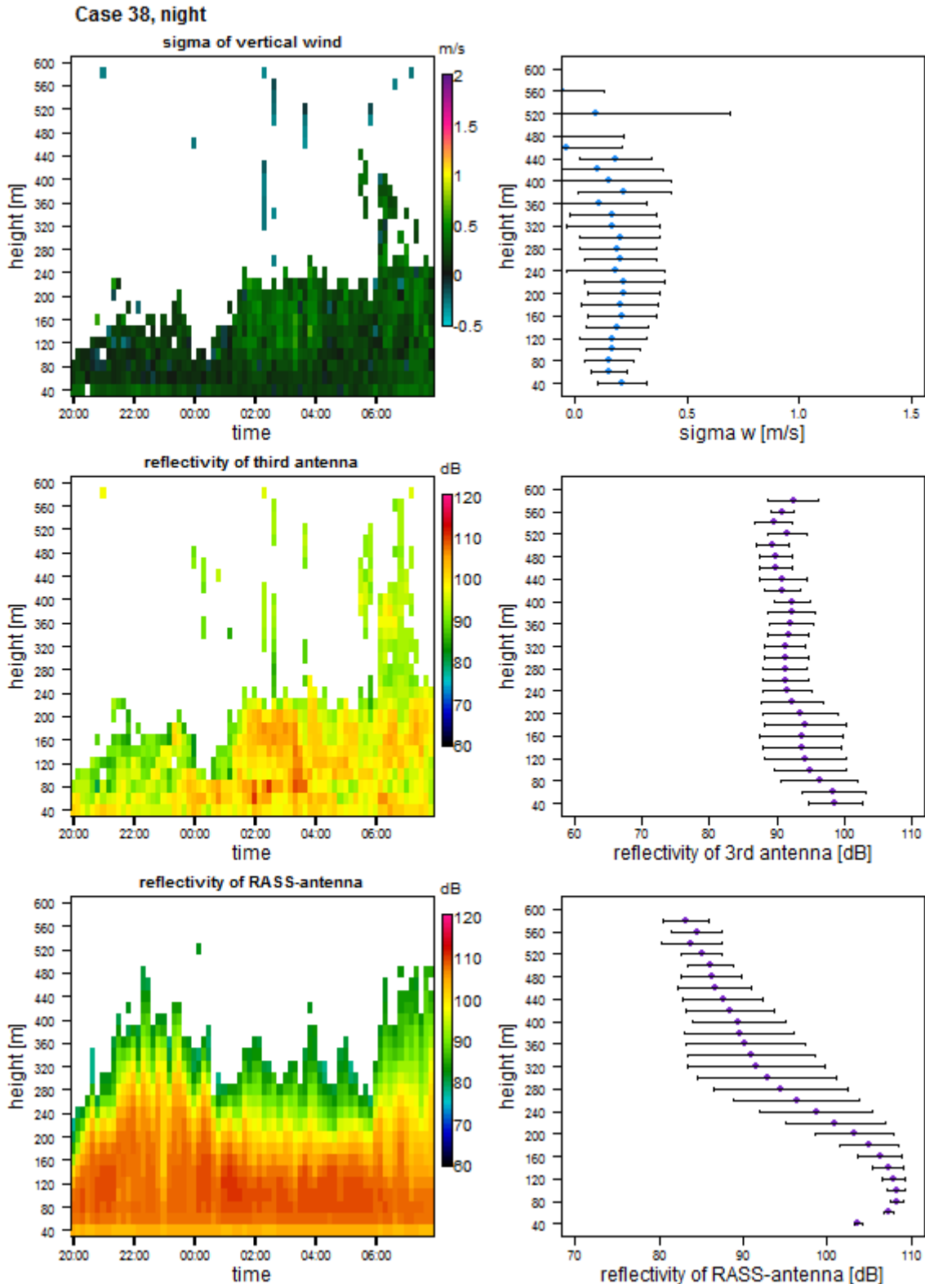


Figure 36: Case 38, part 2 (n = 2) – On the left: ensemble-averaged time-height plots, on the right: height profile with standard deviation

Case 38 was classified as: direction: east; difference of direction: present; wind speed: weak; stratification: stable.

In case 38 there is a change of wind direction from East at the bottom to South at a height of 480 m agl, the standard deviation is relatively high. The wind speeds are low, they increase from  $1 \text{ ms}^{-1}$  at the bottom to only  $4 \text{ ms}^{-1}$  at a height of 500 m agl. The sigma of the vertical wind is very low. The temperature increases from  $19 \text{ }^{\circ}\text{C}$  at the bottom to  $22 \text{ }^{\circ}\text{C}$  at a height of 420 m agl. This means the atmosphere is stratified stable. The reflectivity of the third antenna stays on a very high level, it decreases from 98 dB at the bottom to 92 dB at a height of 580 m agl.

In case 38, as well as in case 22, the counter radiation is very high and the net longwave radiation is low. But in this case, there are very low wind speeds and a rather high temperature.

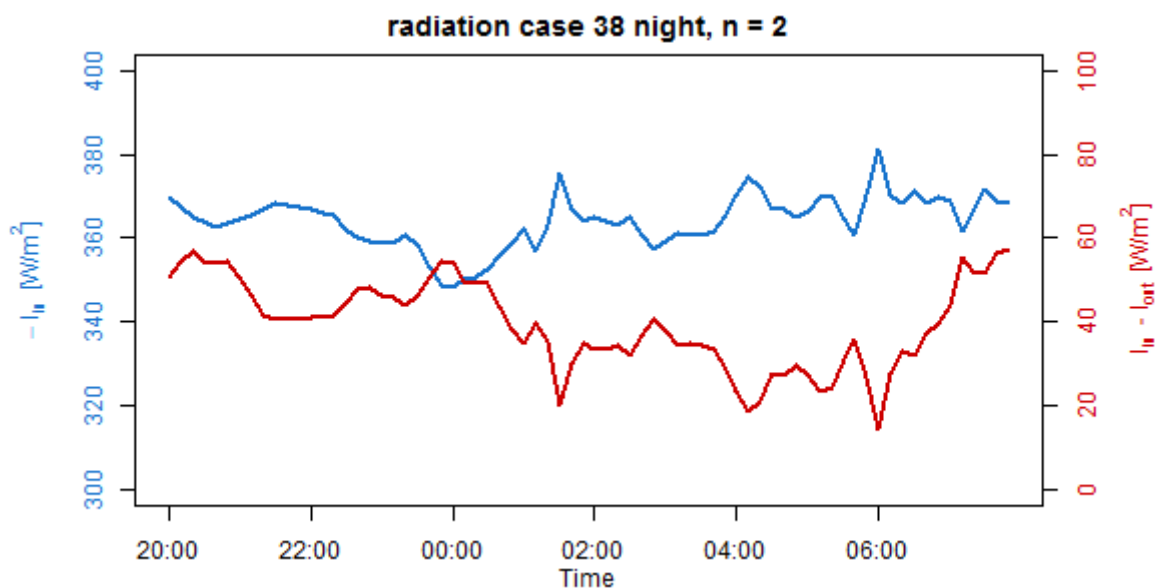


Figure 37: Case 38 – downwelling longwave radiation ( $I_{in}$ ) and net longwave radiation ( $I_{in} - I_{out}$ )

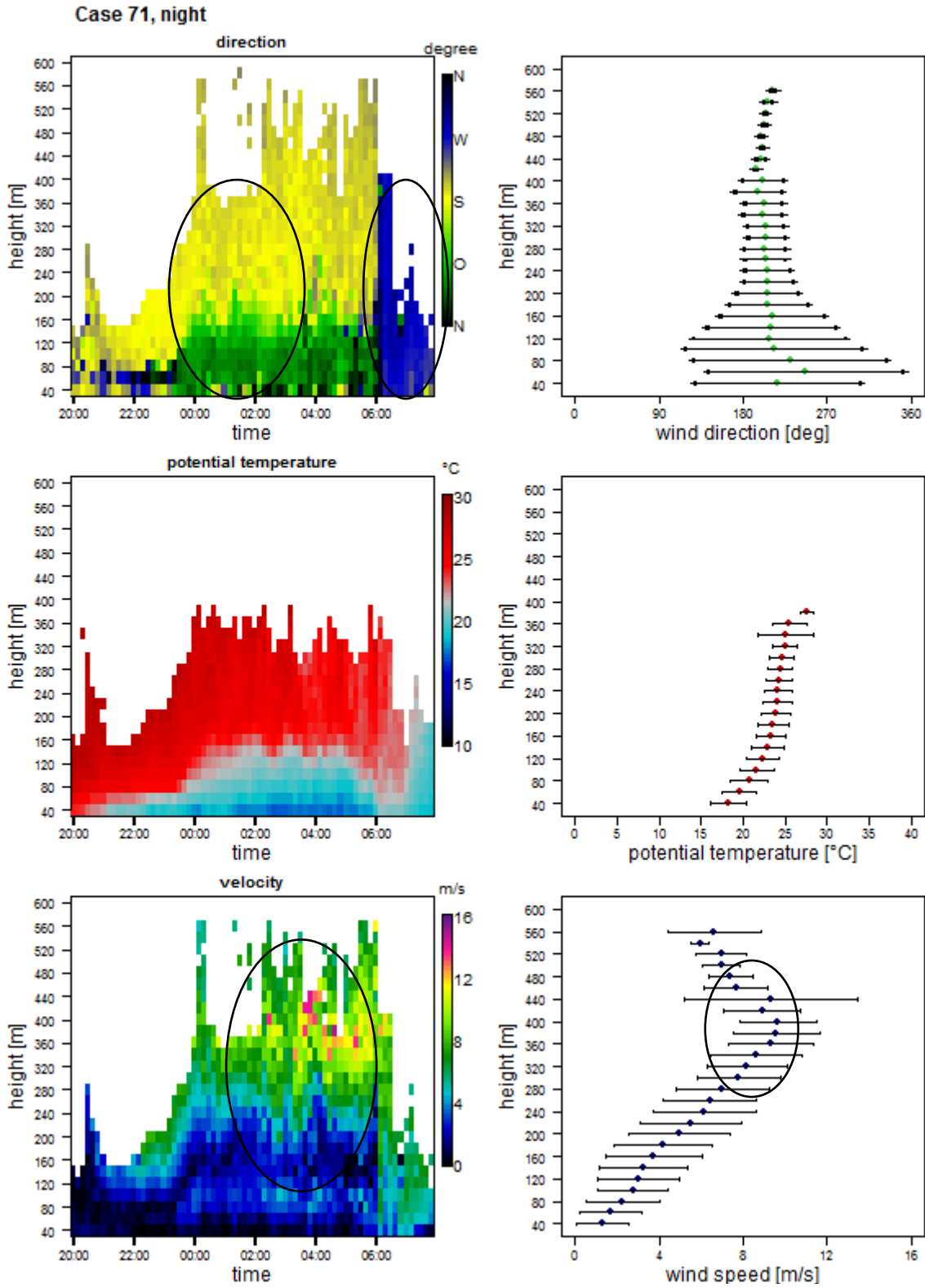


Figure 38: Case 71, part 1 (n = 2) – On the left: ensemble-averaged time-height plots, on the right: height profile with standard deviation

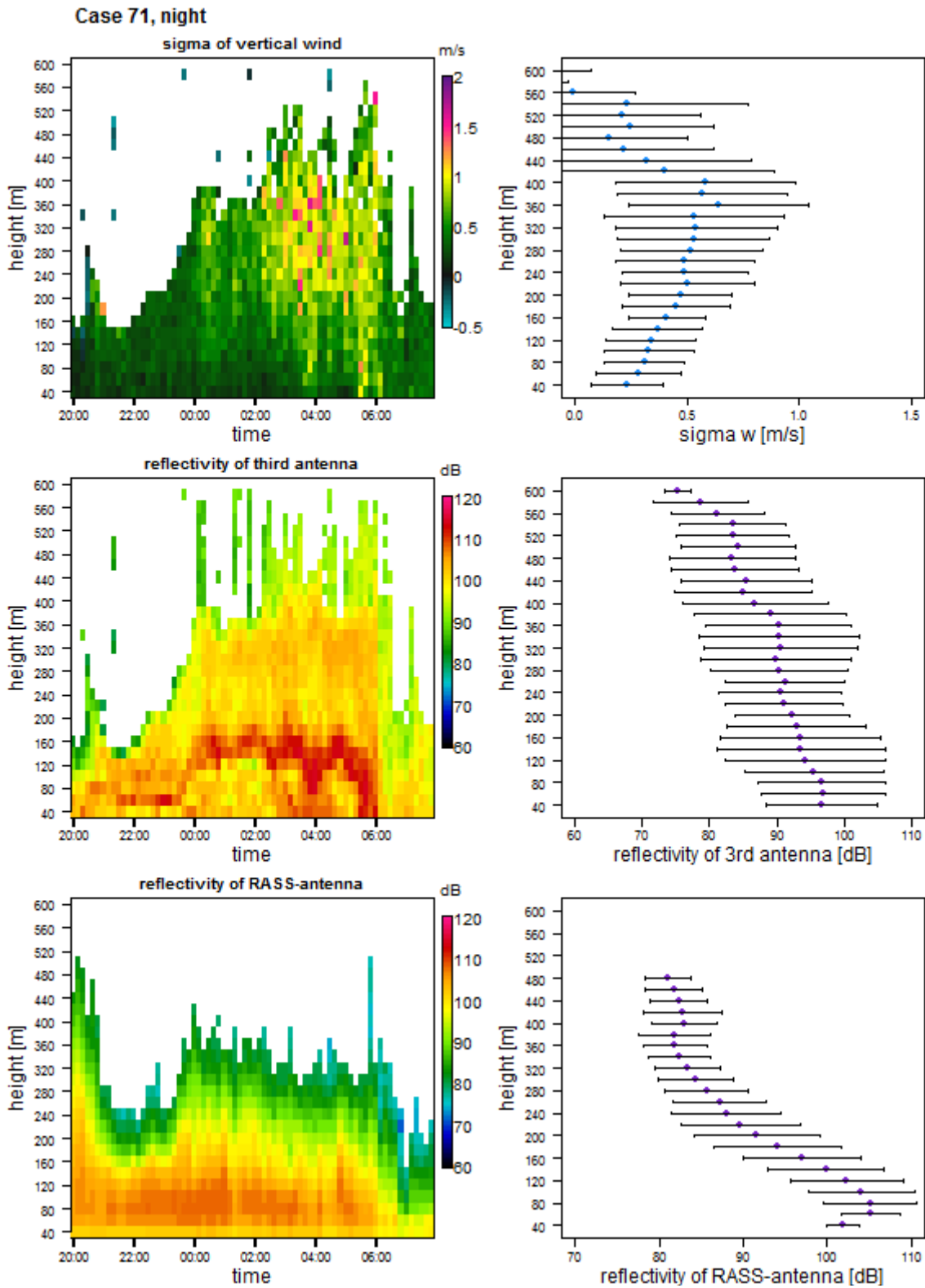


Figure 39: Case 71, part 2 (n = 2) – On the left: ensemble-averaged time-height plots, on the right: height profile with standard deviation

Case 71 was classified as: direction: not differentiated; difference of direction: present; wind speed: not differentiated; stratification: stable.

In case 71 there is a distinct change of the wind direction evident from 23:00 until 06:00. It changes from East in the lower 140 m to South above 140 m agl. After 06:00 the wind direction changes to West over the whole height profile (marked with two circles in the ensemble-averaged time-height plot for the wind direction in Figure 38). The temperature profile shows a distinct stable stratification. The temperature increases from 18 °C at the bottom to 28 °C at a height of 380 m agl. In the profile of the velocity a pronounced low-level jet is visible (marked with a circle in the ensemble-averaged time-height plot for the wind speed in Figure 38). The wind speed increases from 1 ms<sup>-1</sup> at the bottom to 9 ms<sup>-1</sup> at a height of 400 m agl. Above, it decreases to 6 ms<sup>-1</sup> at a height of 560 m agl. This “elbow” indicates a low-level jet with high wind speeds and lower wind speeds above and beneath (marked with a circle in the height profile for the wind speed in Figure 38).

In case 71, the net longwave radiation is about 85 Wm<sup>-2</sup>, which is very high, and decreases slightly until 00:00 and then decreases abruptly, while the counter radiation increases abruptly at 00:00. This is consistent with the building up of the low-level jet, the stable stratification and the difference of the wind direction in Figure 38. At 06:00, the counter radiation increases abruptly again, together with a decreasing net longwave radiation. This corresponds to the abruptly ceasing low-level jet and the change of the wind direction to west.

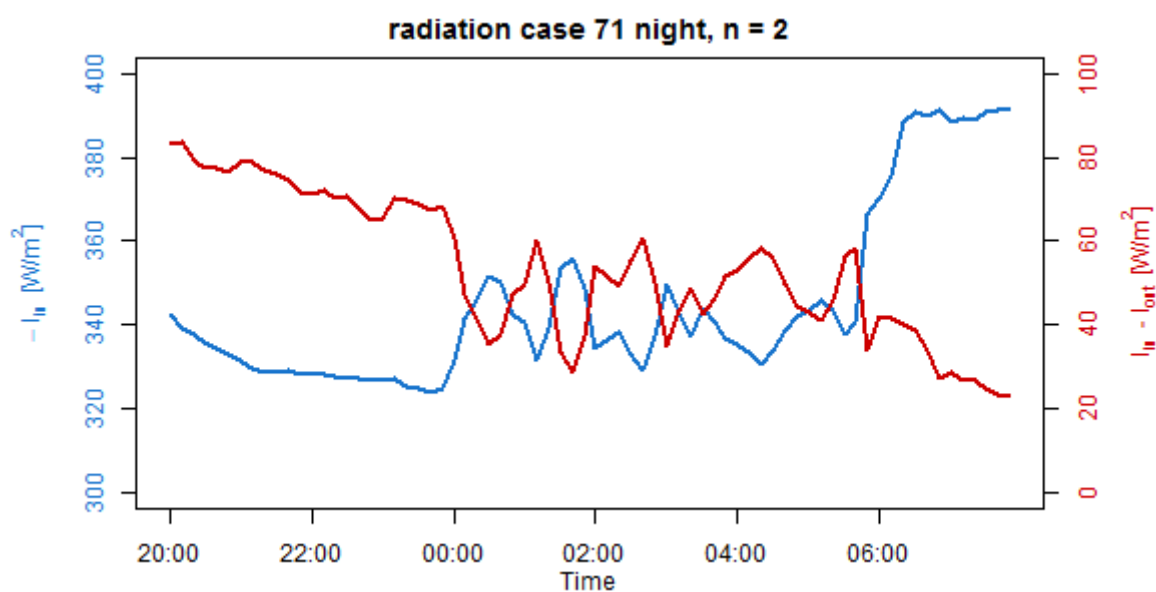


Figure 40: Case 71 – downwelling longwave radiation ( $l_{in}$ ) and net longwave radiation ( $l_{in} - l_{out}$ )

## 6. Interpretation and Discussion

---

As expected, in almost half of the cases (6 of the 10 cases that were selected and analyzed, containing 24 of the 40 nights and 17 of the 40 days) have “West” as the mean wind direction. Considering the fact, that a two-thirds majority was needed to be classified as “West”, there may be some additional days and nights which are classified as “not differentiated” although they mostly have a wind direction of “West”. As Germany is located in the zone of the Westerlies, westerly winds are not surprising. The height profile and the ensemble-averaged time-height plot of case 38 and the ensemble-averaged time-height plot of case 71 show a clear change from east wind to south wind and they are classified as present change of direction. This indicates that the wind at the bottom is coming from the “open” side of the Weißenstädter Basin, where no mountains block the airflow. Above, at about 180 m height agl (case 71) or 320 m agl (case 38) respectively, the wind is coming from the direction of the Schneeberg. Although these cases contain only 4 of the 40 nights, it could be that with a longer measuring period there would be more nights with this pattern of wind direction.

The stratification during the days is neutral in the cases 6 and 56 and slightly stable in case 4 as can be seen in the height profiles. As expected, during the nights, the cases are almost all classified as stable, except case 22, which was classified as not differentiated for the stratification. The stable stratification can be seen clearly in the height profiles, too. This matches with the formation of a stable boundary layer during the night which was explained in the introduction. In case 13 and 15, even a clear inversion layer is visible. In case 22, the lapse rate is almost zero, due to the strong mesoscale wind. Mixing in the air produces an almost uniform temperature distribution. Especially during the nights the air is rather cold with 15 to 17 °C at 40 m above the ground. This could indicate a cold air flow coming from the Schneeberg which is located to the south combined with the radiative cooling of the surface. The temperature near the ground was not evaluated, therefore a clear statement cannot be made, but the process could be similar to the observations of Viana et al. (2012). Viana et al. observed slope flows, gravity waves, and low-level jet using data from a DSDPA.90-24 METEK SODAR RASS and from in-situ measurements (such as sonic anemometer data and high-resolution pressure series from microbarometers) from the SABLES 2006 field campaign (Stable Atmospheric Boundary Layer Experiment in Spain). The field campaign took place in

the Duero basin, surrounded by mountain ranges. They observed the building of a nightly inversion induced by cold air flow from the surrounding slopes combined with the cooling of the surface. During most of the nights a strong cooling of the surface was detected which led to the formation of moderate to strong surface-based thermal inversions.

The wind speed during the days is high with a rather heterogeneous distribution of wind speeds with no clearly visible pattern in the ensemble-averaged time-height plots and an increasing wind speed from ground level upwards in the height profiles in case 6 and 4, which are classified as “strong” winds. The low wind speed at the ground comes from the frictional drag at the surface, the increasing wind speed above could come from synoptic winds that are blowing from greater high-pressure systems to low-pressure systems. As stated in 1.1, in the mixing layer there is also mixing of momentum, which could lead to the heterogeneous distribution of the wind speed. In case 56 the wind speed is generally low, ranging between 0 and 4  $\text{ms}^{-1}$ . During the nights, in one case, case 22, the wind speed is very high because of strong mesoscale winds with an almost linear increase of speed until 12  $\text{ms}^{-1}$ . In another case, case 38, the wind speed is very low, ranging between 0 and 4  $\text{ms}^{-1}$ . In the other 5 cases, case 13, 15, 65, 18 and 71, there is a slightly logarithmic increase up to 12  $\text{ms}^{-1}$  in the height profiles with a clearly stratified velocity distribution in the ensemble-averaged time-height plots. This velocity distribution indicates a low-level jet forming above the stable boundary layer. The stable boundary layer is strongly reducing the friction at the ground allowing almost geostrophic winds, i.e. winds that are not influenced by the frictional drag, near to the surface. Soler et al. (2004) studied air flow in a complex terrain in Spain in the province of Barcelona. The area is a basin called “La Plana de Vic”, surrounded almost completely by mountains with only two narrow channels connecting it to the neighboring areas. Soler et al. are focusing on the distribution of air pollutants. A wide industrial zone is located close to “La Plana”, thus a pollutant flux could affect this region. For the studies a Scintec Doppler SODAR was used. They also detected low-level jets in a height of 100 m during the first hours of the night or in a height of 200 m with a calm layer beneath some hours before sunrise respectively. They connected low wind speeds near the ground to drainage winds coming from the nearby mountains.

Walley (2013) used the same method to classify nights into different classes except that visual indicators were used for the classification and not threshold values as were used in this study. The aim of the Valley Circulation Experiment (VALCEX) was to determine a connection

between two stations in a valley in the H.J. Andrews Experimental Forest in Oregon, one at the beginning of the valley and one at the outflow. At both stations a METEK SODAR and a sonic anemometer were used to collect data. It was found out, that when the wind was blowing along-valley from the upper station to the lower station, the stations were connected and showed similar wind speeds and directions. When the wind was blowing perpendicular to the valley, the stations were not connected. A connection like this wasn't found in the case of this study, not only because the maximum observational height wasn't high enough but also because station 1 and 2 were not laying in such a narrow valley but on top and at the foot of the Schneeberg. But an influence of the Schneeberg was found nevertheless. During the nights of case 15 and 18, there are patches of wind from the south in the ensemble-averaged time-height plots which are showing west wind. This indicates air flowing downslope from the Schneeberg which is located to the south of station 2.

## 7. Conclusion

---

As expected, in the nights with low wind speeds, the formation of a stable boundary layer was detected with the SODAR RASS at station 2. In some nights an inversion was identified, too. When the wind speed was high, the formation of the stable boundary layer was disturbed, resulting in neutral stratification with a uniform temperature distribution. During the days the temperature profile was mostly adiabatic. The direct influence of the Schneeberg could not be detected soundly, mostly the wind blew from west and was not coming from or blowing to the Schneeberg. Except for some small patches that showed southern winds where the rest of the plot showed west wind. In the ensemble-averaged time-height plots. In some cases though a decoupling was observed. At low wind speeds the wind in some nights was coming from the east in the first 100 to 120 m agl and from the south above 120 m agl.

Considering the results for the different cases, it would be reasonable to merge the cases 6 and 4. The distinguishing criteria do not show enough differences for these two cases to allow a differentiation. Case 15 and 18 would also be merged. Here, too, the criteria do not show enough differences.

For the detection of cold air flow from the Schneeberg located in the south, the evaluation of the temperature near the ground would have been great. The SODAR RASS starts measuring

at 40 m above the ground, which is too high to detect cold air flow. The weather station next to the SODAR RASS would provide data including the temperature. This could be used for further analyzation.

The measuring period was only a snapshot, but interesting patterns have been found. Analyzing the data of a longer time period would maybe give better significance with higher numbers of days and nights for the different cases.

The maximum observational height was surprisingly low. It may be useful to try more settings changing the frequency, the measuring height and the orientation to increase the maximum observational height. It could be that the road "wun2", which runs in a distance of 278.5 m caused too much noise and disturbed the measurements. A location further away from such noise sources would be recommendable.

## Literature

---

Geiger, Rudolf; Aron, Robert H.; Todhunter, Paul (2009): *The climate near the ground*. 7th ed. Lanham, Md: Rowman & Littlefield.

Malberg, Horst (2007): *Meteorologie und Klimatologie. Eine Einführung*. Fünfte, erweiterte und aktualisierte Auflage. Berlin, Heidelberg: Springer-Verlag Berlin Heidelberg. Online available at <http://dx.doi.org/10.1007/978-3-540-37222-6>.

Metek, Meteorologische Messtechnik GmbH (1999): *MERASS. The METEK Radio Acoustic Sounding System. Theory of Operation*. Elmshorn, Germany.

Oke, T. R. (1978): *Boundary layer climates*. London: Methuen.

Scintec AG (2016): *Theory Manual*. Scintec Flat Array Sodars SFAS, MFAS, XFAS. 1.01. Aufl. Rottenburg, Germany.

Singal, S. P. (Hg.) (1997): *Acoustic Remote Sensing Applications*. Berlin, Heidelberg: Springer (Lecture Notes in Earth Sciences, 69). Online available at <http://dx.doi.org/10.1007/BFb0009557>.

Soler, M. R.; Hinojosa, J.; Bravo, M.; Pino, D.; Vilà-Guerau de Arellano, J. (2004): Analyzing the basic features of different complex terrain flows by means of a Doppler Sodar and a numerical model. Some implications for air pollution problems. In: *Meteorol Atmos Phys* 85 (1-3). DOI: 10.1007/s00703-003-0041-z.

Stull, Roland B. (2009): *An introduction to boundary layer meteorology*. Reprinted. Dordrecht: Springer (Atmospheric and oceanographic sciences library, 13).

Viana, Samuel; Yagüe, Carlos; Maqueda, Gregorio (2012): Vertical structure of the stable boundary layer detected by RASS-SODAR and in-situ measurements in SABLES 2006 field campaign. In: *Acta Geophysica* 60 (5), S. 1261–1286. DOI: 10.2478/s11600-011-0072-7.

Walley, Jerilyn (2013): *Valley Circulation Experiment: A Classification of Wind Flow in the H. J. Andrews Experimental Forest*, last checked on 06.11.2016.

Whiteman, Charles David (2000): *Mountain meteorology. Fundamentals and applications*. New York: Oxford University Press. Online available at <http://site.ebrary.com/lib/alltitles/docDetail.action?docID=10273240>.

Wiedersich, Berthold (Hg.) (2003): *TaschenAtlas Wetter. Die turbulente Atmosphäre der Erde*. 1. Aufl. Gotha: Klett-Perthes.

## Appendix A: Additional tables and figures

**Table 3: Calculation of the classification for the different days starting with the 1<sup>st</sup> of July as day 1 and ending with the 9<sup>th</sup> of August as day 40**

Day	Direction			Dif. of dir.			Velocity			Stratification		
	1	2	3	1	2	3	1	2	3	1	2	3
1	53	0	14	16	13		7	60		34	11	
2	59	0	7	36	16		4	62		56	4	
3	64	1	7	39	20		6	66		53	10	
4	53	0	16	7	21		25	44		38	4	
5	69	0	3	30	23		2	70		44	14	
6	64	0	8	34	29		0	72		49	10	
7	55	0	15	13	30		10	60		41	9	
8	48	2	21	19	19		9	62		35	12	
9	61	0	11	23	24		1	71		42	10	
10	25	0	39	10	18		25	39		29	5	
11	60	0	3	20	17		3	60		24	13	
12	57	0	3	15	14		20	40		30	3	
13	56	1	6	10	28		17	46		29	10	
14	36	0	34	34	36		8	62		50	11	
15	69	0	3	51	21		4	68		68	3	
16	69	0	3	34	21		2	70		64	4	
17	56	0	11	28	20		11	56		57	2	
18	53	0	15	38	21		7	61		50	13	
19	22	1	37	12	29		40	20		45	7	
20	19	15	32	7	37		49	17		43	9	
21	48	6	10	24	27		34	30		38	20	
22	1	52	16	20	30		29	40		54	2	
23	10	42	15	14	34		38	29		53	1	
24	4	21	33	12	38		49	9		46	8	
25	13	12	35	10	19		53	7		34	1	
26	0	35	17	5	9		42	10		12	4	
27	38	11	21	25	31		35	35		44	13	
28	65	1	6	30	21		18	54		45	9	
29	71	0	0	37	12		1	70		44	5	
30	68	0	2	32	13		11	59		39	6	
31	52	4	15	24	19		21	50		34	11	
32	60	0	4	21	25		13	51		41	4	
33	68	0	4	38	32		4	68		58	10	
34	69	0	3	49	20		8	64		31	38	
35	21	0	19	16	6		11	29		22	2	
36	48	0	21	22	20		8	61		31	10	
37	64	0	7	25	24		6	65		46	2	
38	72	0	0	39	23		8	64		47	16	
39	69	0	2	38	14		1	70		37	13	
40	33	3	33	24	28		37	32		46	4	

Table 4: Sum of the days for all cases

Case	Direction	Dif. of dir	Wind speed	Stratification	# of days
1	West	Absent	Weak	Neutral	0
2	West	Present	Weak	Neutral	0
3	West	ND	Weak	Neutral	0
4	West	Absent	Strong	Neutral	6
5	West	Present	Strong	Neutral	2
6	West	ND	Strong	Neutral	18
7	West	Absent	ND	Neutral	0
8	West	Present	ND	Neutral	1
9	West	ND	ND	Neutral	1
10	West	Absent	Weak	Stable	0
11	West	Present	Weak	Stable	0
12	West	ND	Weak	Stable	0
13	West	Absent	Strong	Stable	0
14	West	Present	Strong	Stable	0
15	West	ND	Strong	Stable	0
16	West	Absent	ND	Stable	0
17	West	Present	ND	Stable	0
18	West	ND	ND	Stable	0
19	West	Absent	Weak	ND	0
20	West	Present	Weak	ND	0
21	West	ND	Weak	ND	0
22	West	Absent	Strong	ND	1
23	West	Present	Strong	ND	0
24	West	ND	Strong	ND	1
25	West	Absent	ND	ND	0
26	West	Present	ND	ND	0
27	West	ND	ND	ND	1
28	East	Absent	Weak	Neutral	0
29	East	Present	Weak	Neutral	0
30	East	ND	Weak	Neutral	1
31	East	Absent	Strong	Neutral	0
32	East	Present	Strong	Neutral	0
33	East	ND	Strong	Neutral	0
34	East	Absent	ND	Neutral	0
35	East	Present	ND	Neutral	1
36	East	ND	ND	Neutral	1
37	East	Absent	Weak	Stable	0
38	East	Present	Weak	Stable	0
39	East	ND	Weak	Stable	0
40	East	Absent	Strong	Stable	0
41	East	Present	Strong	Stable	0
42	East	ND	Strong	Stable	0
43	East	Absent	ND	Stable	0
44	East	Present	ND	Stable	0

45	East	ND	ND	Stable	0
46	East	Absent	Weak	ND	0
47	East	Present	Weak	ND	0
48	East	ND	Weak	ND	0
49	East	Absent	Strong	ND	0
50	East	Present	Strong	ND	0
51	East	ND	Strong	ND	0
52	East	Absent	ND	ND	0
53	East	Present	ND	ND	0
54	East	ND	ND	ND	0
55	ND	Absent	Weak	Neutral	0
56	ND	Present	Weak	Neutral	3
57	ND	ND	Weak	Neutral	1
58	ND	Absent	Strong	Neutral	0
59	ND	Present	Strong	Neutral	0
60	ND	ND	Strong	Neutral	0
61	ND	Absent	ND	Neutral	0
62	ND	Present	ND	Neutral	0
63	ND	ND	ND	Neutral	2
64	ND	Absent	Weak	Stable	0
65	ND	Present	Weak	Stable	0
66	ND	ND	Weak	Stable	0
67	ND	Absent	Strong	Stable	0
68	ND	Present	Strong	Stable	0
69	ND	ND	Strong	Stable	0
70	ND	Absent	ND	Stable	0
71	ND	Present	ND	Stable	0
72	ND	ND	ND	Stable	0
73	ND	Absent	Weak	ND	0
74	ND	Present	Weak	ND	0
75	ND	ND	Weak	ND	0
76	ND	Absent	Strong	ND	0
77	ND	Present	Strong	ND	0
78	ND	ND	Strong	ND	0
79	ND	Absent	ND	ND	0
80	ND	Present	ND	ND	0
81	ND	ND	ND	ND	0

Table 5: Calculation of the classification for the different nights starting with the night of 1<sup>st</sup> to 2<sup>nd</sup> July as night 1 and ending with the night of 9<sup>th</sup> to 10<sup>th</sup> August as night 40

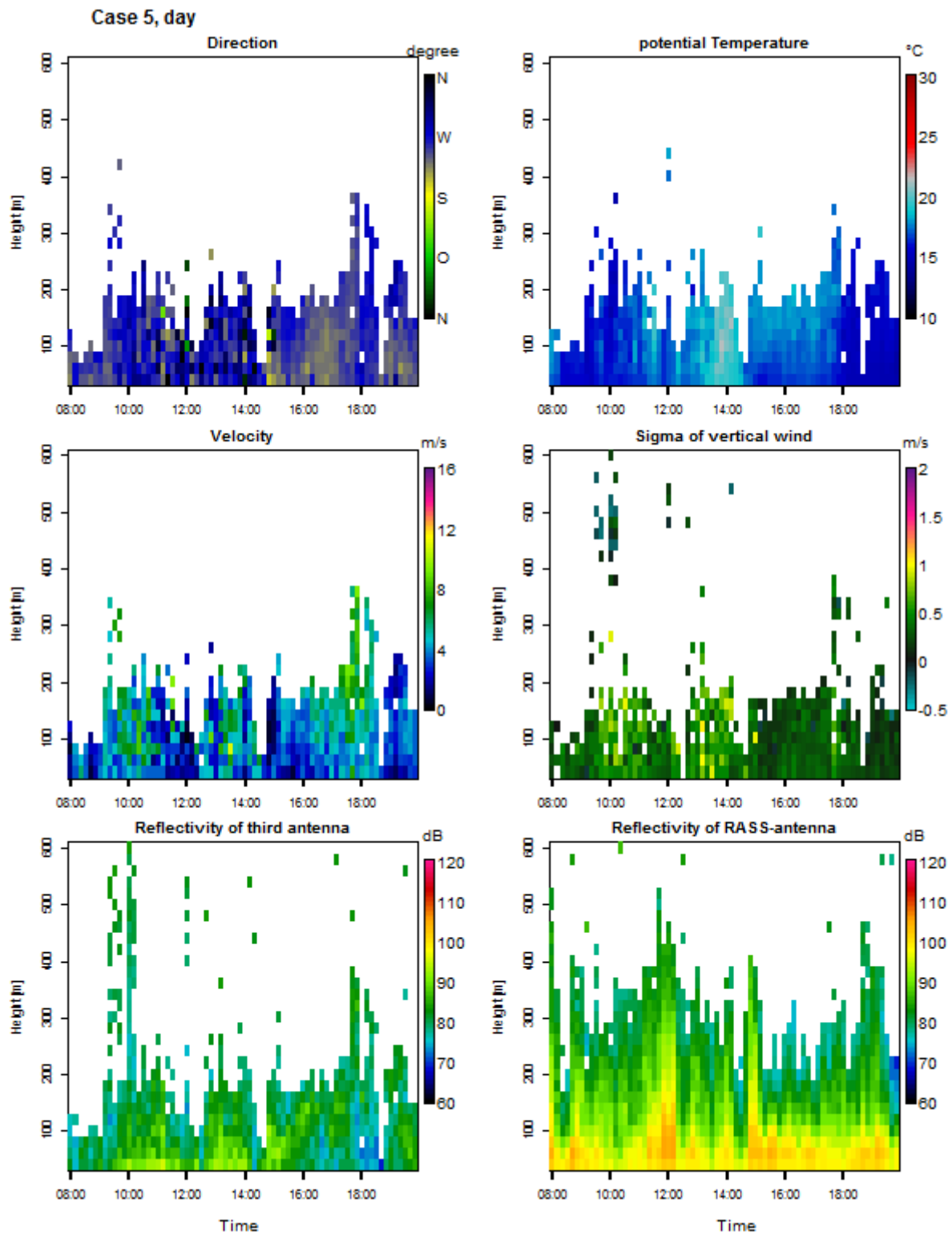
Night	Direction			Dif. of dir.			Velocity			Stratification		
	1	2	3	1	2	3	1	2	3	1	2	3
1	29	11	32	15	36		46	26		2	52	
2	71	0	1	65	2		8	64		8	49	
3	68	0	4	38	23		24	48		3	59	
4	9	12	51	22	40		48	24		2	63	
5	70	0	2	62	5		0	72		43	23	
6	65	0	6	16	42		37	34		1	57	
7	16	18	38	9	41		65	7		0	52	
8	69	0	3	66	5		0	72		8	51	
9	64	1	7	28	34		33	39		1	61	
10	34	0	38	66	5		0	72		0	69	
11	69	0	3	60	3		6	66		40	24	
12	66	0	3	40	4		13	56		5	40	
13	40	0	7	19	13		2	45		17	19	
14	72	0	0	69	3		0	72		2	70	
15	72	0	0	13	55		4	68		5	62	
16	58	0	14	19	50		17	55		7	63	
17	64	0	8	43	28		5	67		9	63	
18	38	10	24	1	63		69	3		0	64	
19	0	63	9	11	61		31	41		0	72	
20	11	35	26	9	48		33	39		0	61	
21	52	6	12	19	39		37	33		0	56	
22	0	53	19	40	20		27	45		0	61	
23	5	42	24	8	55		71	0		2	61	
24	19	17	27	1	10		63	0		0	15	
25	24	22	25	1	59		70	1		0	60	
26	5	36	28	2	45		66	3		0	47	
27	47	8	14	19	30		34	35		0	49	
28	68	0	4	42	22		1	71		4	61	
29	65	0	7	48	14		5	67		1	61	
30	18	20	30	17	22		67	1		0	41	
31	43	0	28	28	24		18	53		9	43	
32	35	6	31	10	48		56	16		0	58	
33	72	0	0	60	0		0	72		34	26	
34	56	0	16	68	3		1	71		0	71	
35	17	2	30	17	11		15	34		13	20	
36	67	0	4	24	38		36	35		3	56	
37	68	0	4	32	27		9	63		2	56	
38	66	0	6	49	22		29	43		1	69	
39	22	12	31	24	15		42	23		4	35	
40	3	24	37	10	38		61	3		28	20	

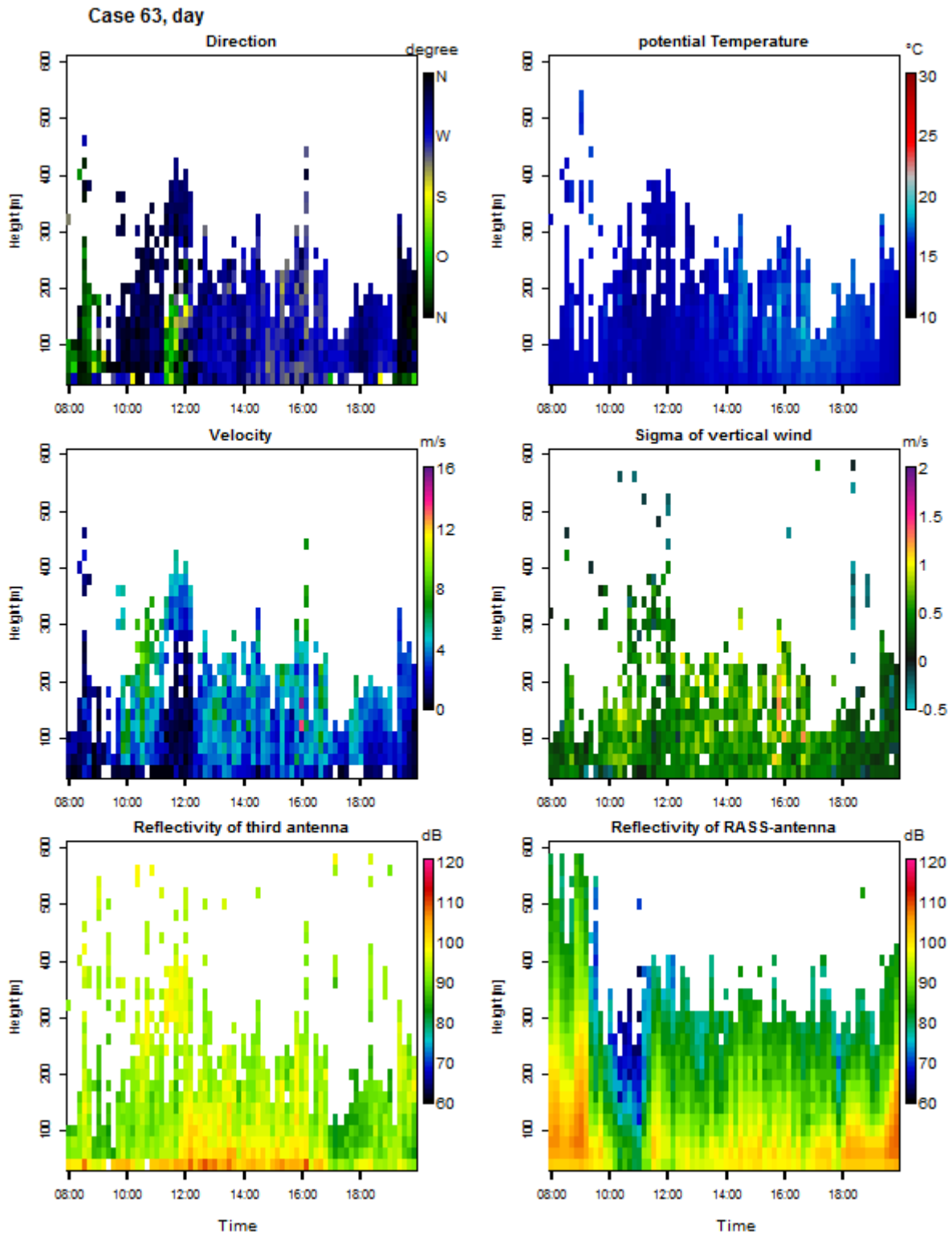
Table 6: Sum of the nights for all cases

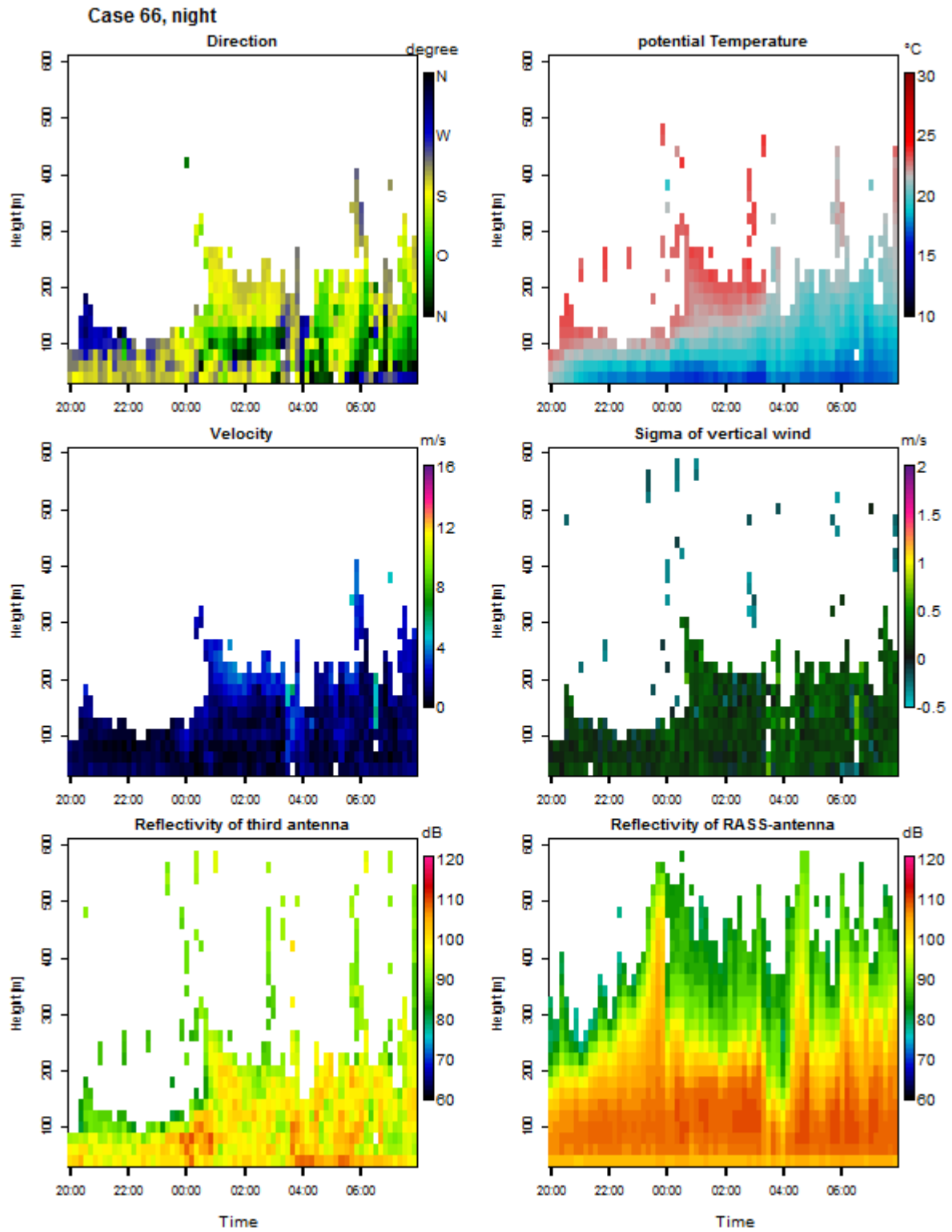
Case	Direction	Dif. of dir	Wind speed	Stratification	# of nights
1	West	Absent	Weak	Neutral	0
2	West	Present	Weak	Neutral	0
3	West	ND	Weak	Neutral	0
4	West	Absent	Strong	Neutral	0
5	West	Present	Strong	Neutral	0
6	West	ND	Strong	Neutral	0
7	West	Absent	ND	Neutral	0
8	West	Present	ND	Neutral	0
9	West	ND	ND	Neutral	0
10	West	Absent	Weak	Stable	0
11	West	Present	Weak	Stable	1
12	West	ND	Weak	Stable	0
13	West	Absent	Strong	Stable	6
14	West	Present	Strong	Stable	2
15	West	ND	Strong	Stable	5
16	West	Absent	ND	Stable	1
17	West	Present	ND	Stable	2
18	West	ND	ND	Stable	3
19	West	Absent	Weak	None	0
20	West	Present	Weak	ND	0
21	West	ND	Weak	ND	0
22	West	Absent	Strong	ND	3
23	West	Present	Strong	ND	0
24	West	ND	Strong	ND	1
25	West	Absent	ND	ND	0
26	West	Present	ND	ND	0
27	West	ND	ND	ND	0
28	East	Absent	Weak	Neutral	0
29	East	Present	Weak	Neutral	0
30	East	ND	Weak	Neutral	0
31	East	Absent	Strong	Neutral	0
32	East	Present	Strong	Neutral	0
33	East	ND	Strong	Neutral	0
34	East	Absent	ND	Neutral	0
35	East	Present	ND	Neutral	0
36	East	ND	ND	Neutral	0
37	East	Absent	Weak	Stable	0
38	East	Present	Weak	Stable	2
39	East	ND	Weak	Stable	0
40	East	Absent	Strong	Stable	0
41	East	Present	Strong	Stable	0
42	East	ND	Strong	Stable	0
43	East	Absent	ND	Stable	1
44	East	Present	ND	Stable	1

45	East	ND	ND	Stable	0
46	East	Absent	Weak	ND	0
47	East	Present	Weak	ND	0
48	East	ND	Weak	ND	0
49	East	Absent	Strong	ND	0
50	East	Present	Strong	ND	0
51	East	ND	Strong	ND	0
52	East	Absent	ND	ND	0
53	East	Present	ND	ND	0
54	East	ND	ND	ND	0
55	ND	Absent	Weak	Neutral	0
56	ND	Present	Weak	Neutral	0
57	ND	ND	Weak	Neutral	0
58	ND	Absent	Strong	Neutral	0
59	ND	Present	Strong	Neutral	0
60	ND	ND	Strong	Neutral	0
61	ND	Absent	ND	Neutral	0
62	ND	Present	ND	Neutral	0
63	ND	ND	ND	Neutral	0
64	ND	Absent	Weak	Stable	0
65	ND	Present	Weak	Stable	4
66	ND	ND	Weak	Stable	2
67	ND	Absent	Strong	Stable	1
68	ND	Present	Strong	Stable	0
69	ND	ND	Strong	Stable	0
70	ND	Absent	ND	Stable	0
71	ND	Present	ND	Stable	2
72	ND	ND	ND	Stable	1
73	ND	Absent	Weak	ND	0
74	ND	Present	Weak	ND	1
75	ND	ND	Weak	ND	0
76	ND	Absent	Strong	ND	0
77	ND	Present	Strong	ND	0
78	ND	ND	Strong	ND	1
79	ND	Absent	ND	ND	0
80	ND	Present	ND	ND	0
81	ND	ND	ND	ND	0

Additional Plots for cases 5, 63 and 66, which were not analyzed in the mean text:







## Appendix B: Documentantation of settings

---

### Settings for the SODAR RASS:

Name of the parameter settings: WOBL5\_Voit\_2000\_600s\_12345R. This was used from the beginning (30.06.16 17:59:23) until 14.07.16 09:40:00.

- Ausgabeparameter (output parameter)
  - o Allgemein (in general):  
Höhe (height), Geschwindigkeit (velocity), Richtung (direction), Geschwindigkeit vektoriell (vectorial velocity): U, V, W, Phi sigma, Diffusion, Temperatur (temperature)
  - o Je Antenne (per antenna) (for antennas 1, 2, 3, 4, 5 and R):  
Spektren (spectra), Reflektivität (reflectivity), Radial (radial), Sigma, Plausibilität (plausibility), S/R-Verhältnis (signal-to-noise ratio)
  - o Geräteerkennung (device identification): SDR
  - o Messhöhen [m] (measuring heights [m]):  
40 to 780 in 20 m steps, 795, 910, 930
  - o Zeitzone (time zone): MEZ
  - o Momentanwerte (instantaneous values) (for antennas 1, 2, 3, 4, 5 and R):  
Höhe (height), Spektren (spectra), Reflektivität (reflectivity), Radial (radial), Plausibilität (plausibility), S/R-Verhältnis (signal-to-noise ratio)
- Geräteparameter
  - o Messzeit (measuring time): 600 s
  - o Sendefrequenz (transmission frequency): 2000 Hz
  - o Diffusionsklassen-Tabelle (table of stability classes): t7306
  - o Höhenbereich (height range):  
Rauschhöhe (noise height): 900 m  
Maximale Höhe (maximum height): 800 m  
Stufung (spacing): 20 m  
Minimale Höhe (minimum height): 30 m  
Festechounterdrückung bis (suppression of fixed echo until): 0 m
- Dienste:
  - o Sodar mit PC-Zeit synchronisieren (synchronize sodar with pc-time): ja/yes
  - o Zeitstempel durch PC-Zeit ersetzen (replace time stamp with pc time): nein/no
  - o Zeitstempel auf ganze Minuten runden (round time stamp to full minutes): ja/yes

Name of the parameter settings: WOBL5\_Voit\_1600\_600s\_123R. This was used from 14.07.16 09:50:00 until 10.08.16 16:20:00.

- Ausgabeparameter (output parameter)
  - o Allgemein (in general):  
Höhe (height), Geschwindigkeit (velocity), Richtung (direction), Geschwindigkeit vektoriell (vectorial velocity): U, V, W, Phi sigma, Diffusion, Temperatur (temperature)
  - o Je Antenne (per antenna) (for antennas 1, 2, 3 and R):  
Spektren (spectra), Reflektivität (reflectivity), Radial (radial), Sigma, Plausibilität (plausibility), S/R-Verhältnis (signal-to-noise ratio)
  - o Geräteerkennung (device identification): SDR
  - o Messhöhen [m] (measuring heights [m]):  
40 to 580 in 20 m steps, 595, 710, 730
  - o Zeitzone (time zone): MEZ
  - o Momentanwerte (instantaneous values) (for antennas 1, 2, 3, 4, 5 and R):  
Höhe (height), Spektren (spectra), Reflektivität (reflectivity), Radial (radial), Plausibilität (plausibility), S/R-Verhältnis (signal-to-noise ratio)
- Geräteparameter
  - o Messzeit (measuring time): 600 s
  - o Sendefrequenz (transmission frequency): 1600 Hz
  - o Diffusionsklassen-Tabelle (table of stability classes): t7306
  - o Höhenbereich (height range):  
Rauschhöhe (noise height): 700 m  
Maximale Höhe (maximum height): 600 m  
Stufung (spacing): 20 m  
Minimale Höhe (minimum height): 30 m  
Festechounterdrückung bis (suppression of fixed echo until): 0 m
- Dienste:
  - o Sodar mit PC-Zeit synchronisieren (synchronize sodar with pc-time): ja/yes
  - o Zeitstempel durch PC-Zeit ersetzen (replace time stamp with pc time): nein/no
  - o Zeitstempel auf ganze Minuten runden (round time stamp to full minutes): ja/yes

## Acknowledgements

---

My thanks go to my supervisor, Prof. Dr. Christoph Thomas, for the active support and the many helpful comments.

To the micrometeorology group for the help with the set-up and dismanteling of the instruments.

To Jo Olesch for the help with all kind of technical problems.

To Dr. Wolfgang Babel for the second revision.

To Dr. Wolfgang Babel and Lena Pfister for the help with the Program R.

To Sarah Holden for the great teamwork, the moral and active support and for the chocolate.

## Declaration of Authorship

---

I herewith certify that the work presented above with the title “Dynamics of temperature and wind profile in the boundary layer of a valley in the Fichtelgebirge Mountains” is to the best of my knowledge and belief original and the result of my own investigations. Third party work, non-published and published information I received are properly and duly acknowledged. This work has never previously been submitted to any other examination committee.

---

Place, Date

---

Elena Loos